Army Research Laboratory

Turbulence Simulation: Outer Scale Effects on the Refractive Index Spectrum

By
David H. Tofsted

Computational and Informational Sciences Directorate
Battlefield Environment Division

ARL-TR-548 **November 2000**

Approved for public release; distribution unlimited

NOTICES

Disclaimers

The findings in this report are not to be construed as an official Department of the Army position, unless so designated by other authorized documents.

Citation of manufacturers' or trade names does not constitute an official endorsement or approval of the use thereof.

REPORT DOCUMENTATION PAGE

Form Approved
OMB No. 0704-0188

1. AGENCY USE ONLY (*Leave Blank*)	2. REPORT DATE	3. REPORT TYPE AND DATES COVERED
	November 2000	Final

4. TITLE AND SUBTITLE
Turbulence Simulation: Outer Scale Effects on the Refractive Index Spectrum

5. FUNDING NUMBERS

6. AUTHOR(S)

D. Tofsted

7. PERFORMING ORGANIZATION NAME(S) AND ADDRESS(ES)

U.S. Army Research Laboratory
Computational and Informational Sciences Directorate
Battlefield Environment Division
ATTN: AMSRL-CI-EW
White Sands Missile Range, NM 88002-5501

8. PERFORMING ORGANIZATION REPORT NUMBER

ARL-TR-548

9. SPONSORING/MONITORING AGENCY NAME(S) AND ADDRESS(ES)

U.S. Army Research Laboratory
2800 Powder Mill Road
Adelphi, MD 20783-1145

10. SPONSORING/MONITORING AGENCY REPORT NUMBER

ARL-TR-548

11. SUPPLEMENTARY NOTES

12a. DISTRIBUTION/AVAILABILITY STATEMENT

Approved for public release; distribution unlimited.

12b. DISTRIBUTION CODE

A

13. ABSTRACT (Maximum 200 words)

An analysis of the commonly used refractive index power spectrum indicates that its method of simulating outer scale effects is deficient in two aspects: it approaches a nonzero value at zero frequency and is ambiguous regarding definition and usage of the outer scale in its functional form. To resolve these problems, a modified form of the refractive index spectrum is proposed which properly models the behavior of the spectrum at zero frequency and simulates the energy-containing eddy region. In support of this analysis, outer scale is defined such that it is independent of the mathematical form used to describe the refractive index spectrum. Based on reported experimental data, a new equation for outer scale as a function of stability conditions is proposed, revealing dependence of the outer scale on both height above the surface and the stability-related Monin-Obukhov length.

14. SUBJECT TERMS

propagation, optical turbulence, coherence diameter, outer scale, Kolmogorov spectrum, von Karman spectrum.

15. NUMBER OF PAGES
58

16. PRICE CODE

17. SECURITY CLASSIFICATION OF THIS REPORT	18. SECURITY CLASSIFICATION OF THIS PAGE	19. SECURITY CLASSIFICATION OF ABSTRACT	20. LIMITATION OF ABSTRACT
UNCLASSIFIED	UNCLASSIFIED	UNCLASSIFIED	SAR

NSN 7540-01-280-5500

Standard Form 298 (Rev. 2-89)
prescribed by ANSI Std. Z39-18-298-102

Preface

The structural effects of the outer scale of turbulence are significant in certain propagation problems in the Earth's lower atmosphere. In particular, image wander (angle of arrival fluctuations of distant objects) and shape distortion of objects due to nonisoplanatism are critically dependent on the shape of the refractive index power spectrum in its energy-containing-eddy region. To correctly model these effects requires an accurate model of the outer scale of turbulence, both as a function of height and as regards how it impacts the refractive index spectrum.

In the past, the outer scale was defined rather vaguely, using order of magnitude arguments. Or, at best, outer scale was defined based of the mathematical form used in describing the refractive index spectrum itself. Also, the outer scale was often equated with the so-called *mixing length* used in numerical weather model closure methods for solving the Navier-Stokes equations.

But the mixing length is merely a convenient order-of-magnitude length scale. Atmospheric optics has tended to adopt this value in lieu of better parameterizations. This report attempts to fill this data void by dealing with several aspects of the outer scale problem. To accurately determine outer scale effects with regard to propagation problems involving optical turbulence (turbulent image wander, image shape distortion, etc.) better models must be sought than those based on reasonable guesses.

First, I propose a definition for the outer scale which is independent of the particular mathematical form used in describing the refractive index spectrum.

Second, an analysis of temperature spectrum data from the 1968 Kansas experiment is discussed that leads to a new form for the refractive index spectrum. For completeness, I also propose a combined spectrum called the composite spectrum that includes both inner and outer scale influences.

Third, based on the analysis of the spectrum itself, a relationship is determined between the peak frequency data from the Kansas experiment and the outer scale of turbulence. This relationship describes a functional form for the turbulence outer scale as a function of both height above the surface and a surface layer stability parameter, the Monin-Obukhov length.

Acknowledgement

I wish to acknowledge the contributions of the reviewers: Dr. Edgar Andreas of the U.S. Army Cold Regions Research and Engineering Laboratory, Hannover, NH, and Dr. Donald Hoock and Ms. Gail Vaucher of the U.S. Army Research Laboratory. In examining this work and providing helpful insights they have improved both the overall presentation and the chapter 2 integral derivations.

Contents

Figures

Executive Summary

Synopsis

This report considers the nature of the outer scale of turbulence, its relationship to the refractive index power spectrum, and the form of this spectrum based on data reported from the 1968 Kansas experiment [Kaimal *et al.*, 1972].

The outer scale of turbulence is a length scale used to demarcate the beginning of the so-called inertial subrange. For two points separated by distances greater than the so-called inner scale length (a few millimeters) and less than the outer scale length (on the order of meters) fluctuations in refractive index follow a "2/3 law". Difficulties arise for separation distances outside this range. These deviations are the subject of spectral modifications that account for both inner and outer scale variations.

Under many circumstances the influence of the outer scale is not significant. For example, optical turbulence effects on beam propagation generally involve scintillation and beam spread influences that are relatively impervious to outer scale effects due to the limited width of the beam. Imaging of point sources through turbulence is also little affected by outer scale when considering only turbulent blurring and scintillation effects since the optics entrance aperture is smaller than the outer scale.

However, for object jitter and image distortion effects, outer scale influences are likely dominant. The outer scale length has been shown to be directly related to the spatial frequency that has the greatest influence on angle of arrival variations [Tofsted, 1992]. Yet outer scale is not well defined or quantified. To correct deficiencies regarding outer scale effects characterization, this report focuses on three issues: (1) Defining outer scale independent of the particular mathematical form being adopted to describe the refractive index spectrum. (2) Developing a more accurate refractive index spectral form for low spatial frequency characterization. (3) Deriving an equation for evaluating outer scale based on meteorological data measurements.

Results

To define the outer scale of turbulence requires a knowledge of the form the refractive index spectrum assumes when inner and outer scale effects are not considered. This spectrum is called the Kolmogorov spectrum,

$$\Phi_{nK}(\kappa) = 0.033\, C_n^2\, \kappa^{-11/3}, \tag{1}$$

where κ is a spatial frequency variable given in units of radians per meter and C_n^2 is the refractive index structure parameter with units of refractive index squared (unitless) times meters to the -2/3 power.

The Kolmogorov spectrum is the most frequently encountered spectrum in the optical turbulence literature because it has the simplest form. This property makes the Kolmogorov spectrum a useful benchmark, as follows: Assume we identify some refractive index spectral form which accounts for outer scale effects. Call it $\Phi_n(\kappa)$. For κ values within the so-called inertial subrange we will have $\Phi_n(\kappa) \approx \Phi_{nK}(\kappa)$. For κ below this range, one enters the energy-containing-eddy region in which $\Phi_n < \Phi_{nK}$, with the ratio Φ_n/Φ_{nK} approaching zero as κ approaches zero. Within this framework, the outer scale can be defined as,

$$\Phi_n\left(\frac{1}{L_o}\right) = \frac{1}{2}\,\Phi_{nK}\left(\frac{1}{L_o}\right). \tag{2}$$

Though arbitrary, heretofore no quantitative definition has been established. Using this definition, the Kansas 1968 experimental data reported by Kaimal *et al.* [1972] were analyzed. While the goal of the analysis was to evaluate the outer scale length, it was necessary to first produce a new model of the refractive index spectrum for low spatial frequencies, κ. This was necessary because the Kansas data were plotted as one-dimensional (1-D) spectra ($F_n(\kappa_1)$), typical of sensor data collected through meteorological tower measurements, where the wind advects spatially fluctuating air past the tower location. On the other hand, atmospheric turbulence studies are based on three-dimensional (3-D) spectra. The only way to compare the two is to propose a 3-D spectrum and transform it to its 1-D representation, as,

$$F_n(\kappa_1) = 4\,\pi \int_0^\infty \Phi_n\left(\sqrt{\kappa_1^2 + \kappa_r^2}\right)\,\kappa_r\,d\kappa_r. \tag{3}$$

Comparison of spectra led to the development of a relationship between outer scale and the reported peak frequency of a universal function of scalar property fluctuations in turbulent flow. This peak frequency is given in terms of z/L, the dimensionless ratio of height above the surface (z) to the Monin-Obukhov length (L).

Conclusion

Together, the new definition of outer scale developed, the new spectral form to describe the effects of the outer scale on the refractive index spectrum, and the new relationship describing outer scale as a function of height and stability extend the accuracy of modeling low spatial frequency effects dramatically.

1. Introduction

The atmospheric optics community has generally relied on a few select forms for representing refractive index spectra, as illustrated by the following examples. Nelson *et al.* [2000] use a simple Kolmogorov spectrum [Kolmogorov, 1962] that exhibits $\kappa^{-11/3}$ behavior at all spatial frequencies, where κ is a radially symmetric spatial frequency variable given in units of radians per meter. (This spectrum was described in the Executive Summary.) Frehlich [2000] augments the standard Kolmogorov spectrum to account for inner scale effects through the addition of a Hill [1978] Spectrum term which accounts for the peculiar bump phenomenon which occurs in the vicinity of the frequency equivalent of the inner scale length. These studies, and others [Frehlich, 2000; Davis and Walters, 1994; Martin and Flatté, 1988; etc.], focus on beam wave propagation, the goal of which is usually to limit, as much as possible, the horizontal spread of such beams. The narrow cones used in these studies tend to not experience significant outer scale effects. And the phase screens used in propagating the beams are usually centered on the beam path.

Perhaps more sensitive to outer scale effects are studies such as Ellerbroek [1997] and Young *et al.* [1998]. The former uses a von Kármán spectrum referenced to Tatarskii [1971]. The latter uses a modified von Kármán spectrum which includes an inner scale roll off region generally attributed to Tatarskii [1971]. Similarly, Yan *et al.* [2000] used a von Kármán spectrum in their adaptive optics study.

Together, the Kolmogorov spectrum, in combination with von Kármán, Tatarskii, and/or Hill spectral modifiers, generally span the gamut of the available choices of spatial frequency spectra for characterizing optical turbulence. Significant theoretical and experimental work has been accomplished in the high spatial frequency regime, with various representations of this bump effect available [Churnside, 1990; Andrews, 1992; Frehlich, 1992].

All spectra exhibit similar $\kappa^{-11/3}$ dependence for κ within the inertial subrange, and the behavior of the Andrews and Frehlich models are very similar. Of more concern are differences between proposed versions of the von Kármán spectrum. While all models of this spectrum are given as,

$$\Phi_n(\kappa) = \frac{0.033\, C_n^2}{\left(\kappa^2 + \kappa_\odot^2\right)^{11/6}}, \tag{1}$$

there is disagreement over the definition of $\kappa_\odot$ as well as problems with the behavior of this functional form at low spatial frequencies.

For example, Ishimaru [1978], Ellerbroek [1997] and Young *et al.* [1998] define $\kappa_\odot$ as $1/L_o$, where L_o is referred to as the outer scale. But Kopeika [1998] and Clifford [1978] define $\kappa_\odot$ as $2\pi/L_o$, yet also refer to L_o as the outer scale. Obviously two divergent forms of the same equation cannot lead to identical definitions for the outer scale.

Ishimaru indicated L_o should be on the order of the height above the surface in appendix C of his book. Kopeika set L_o to $k_v\, z$, where k_v is von Kármán's constant, equal to approximately 0.385 over rough surfaces [Frenzen and Vogel, 1995], and z is the height above the surface. Combining the uncertainty about the definition of L_o with the uncertainty about the definition of $\kappa_\odot$, we have over an order of magnitude disagreement between Ishimaru and Kopeika regarding the positioning of the outer scale cutoff.

The von Kármán spectrum also has a second problem. At the low frequency limit, as $\kappa \rightarrow 0$, the spectrum should also approach a zero value. The von Kármán spectrum approaches the constant value $0.033\, C_n^2\, \kappa_\odot^{-11/3}$ instead. The zero limit requirement can be shown through the relationship between the refractive index spectrum Φ_n and the spatial autocorrelation function, $\Gamma_n(r)$ [Goodman, 1985], given by,

$$\Gamma_n\left(\vec{r}\right) = \left\langle n'\left(\vec{x}\right)\, n'\left(\vec{x}+\vec{r}\right)\right\rangle . \tag{2}$$

Here, the angle brackets represent an expectation operation, n' represents refractive index perturbations at positions $\vec{x}$ and $\vec{x}+\vec{r}$ about an average refractive index value.

Φ_n is related to Γ_n through a Fourier relationship as will be discussed further in section 2.3. However, because Γ_n is an autocorrelation function of n', Φ_n must be proportional to the magnitude squared of the Fourier transform of n' [cf., Gaskill, 1978]. But n' is a zero mean quantity by definition and hence (Parseval's theorem) n''s Fourier transform must equal zero at the origin. By extension, Φ_n must also equal zero at the origin. Neither the Kolmogorov nor the von Kármán spectra exhibit this property.

Any study purporting to consider optical turbulence effects on image propagation should begin by considering the outer scale influences on the problem because the outer scale represents the size scale with the greatest fluctuation energy in the spectrum. The available energy normally can be measured as a function of $\Phi_n(\kappa)$ times $4\pi\kappa^2\, d\kappa$, the differential volume associated with fluctuations at a particular spatial frequency scale. Since Φ_n is decreasing as $\kappa^{-11/3}$ across the inertial subrange, the combined effect will be the maximum fluctuations that occur somewhere near the outer scale size.

2. Analysis

To address the deficiencies in the existing theory discussed in the introduction, several aspects of optical turbulence related to low spatial frequency phenomena must be considered. A new form for the refractive index spectrum is proposed to replace the currently dominant von Kármán spectrum. Spectral analysis arguments are used to indicate the limiting behavior of the spectrum at low spatial frequency. Analysis of actual data provides further insight into the detailed behavior of the spectrum in the vicinity of the outer scale frequency, $1/L_o$. However, because of ambiguities in definition of the outer scale itself, it is necessary to clarify the meaning of this quantity first and then use this more precise definition in relating the outer scale to measureable meteorological quantities associated with the atmospheric surface layer.

In section 2.1, a new definition of outer scale is proposed. This new definition is linked to a property of the outer-scale-influenced refractive index spectrum itself, rather than to a specific form used in describing that spectrum. In section 2.2, the use of the mixing length is briefly discussed that has led to some confusion in the past. In section 2.3, an analysis is performed to link the research findings for the Kansas experiment to the three-dimensional (3-D) refractive index spectrum. The results of this analysis permit both postulating a new outer scale influenced spectrum and establishing a relationship between outer scale and the Monin-Obukhov length, an atmospheric surface layer stability parameter. The implications of this functional behavior on the refractive index itself will then be considered, along with a discussion in section 2.4 of a composite spectrum that accounts for both inner and outer scale effects.

2.1 Outer Scale Defined

The first step in describing the outer scale effects should be to uniquely identify the outer scale in such a way that it is not dependent on the form of the equation in which it appears. As was discussed in chapter 1, the appearance of the outer scale in the von Kármán spectrum results in an ambiguity based on different literature sources. The same value of outer scale, L_o, has significantly different ramifications when defining $\kappa_\odot = 1/L_o$ [Ishimaru, 1978; Andrews and Phillips, 1998] as opposed to the use of $\kappa_\odot = 2\pi/L_o$ [Clifford, 1978; Kopeika, 1998].

To resolve this dilemma I propose the following: Let $\Phi_{nK}(\kappa)$ represent the Kolmogorov spectrum,

$$\Phi_{nK}(\kappa) = 0.033\, C_n^2\, \kappa^{-11/3}, \tag{3}$$

where κ is a spatial frequency variable with units of radians per meter and C_n^2 is the refractive index structure parameter with units of refractive index squared (unitless) times meters to the -2/3 power. The refractive index spectrum thus has units of volume. Let $\Phi_n(\kappa, \mathcal{L}_o)$ represent any spectrum where outer scale effects are included, and where the parameter $\mathcal{L}_o$ reflects outer scale effects but is not necessarily equal to the outer scale. To quantitatively define the value of the outer scale length, L_o, we need a new variable, $\kappa_\oslash = 1/L_o$. We will define the outer scale as that length which satisfies the relation,

$$\frac{\Phi_n(\kappa_\oslash, \mathcal{L}_o)}{\Phi_{nK}(\kappa_\oslash)} = \frac{1}{2}. \tag{4}$$

Typically, $\mathcal{L}_o$ appears in functional forms describing Φ_n involving only the product $\kappa\mathcal{L}_o$. Due to the way $\mathcal{L}_o$ appears in these functional forms, outer scale parameters in these equations can always be written as linear relations relative to the actual outer scale: $\mathcal{L}_o = \alpha L_o$.

For example, in the case of the von Kármán spectrum, when $\kappa_\odot = 1/\mathcal{L}_o$ is used, we must have α equal to $\left(2^{6/11} - 1\right)^{-1/2} \approx 1.475$. Otherwise, using the definition, $\kappa_\odot = 2\pi/\mathcal{L}_o\ \alpha$ is written as, $2\pi\left(2^{6/11} - 1\right)^{-1/2} \approx 9.269$. In either case L_o maintains the same position relative to the knee of the spectrum regardless of the form adopted for $\kappa_\odot$.

2.2 Outer Scale versus Mixing Length

One hazard to avoid in the available literature is the difference between outer scale and a quantity customarily called the mixing length or the characteristic length. While various mixing length definitions are available, these are usually employed in providing closure mechanisms for solving the Navier Stokes equations [e.g., Lewellen, 1977; Zhao, 1994; Finardi *et al.*, 1995]. In this literature Kopeika's $k_v z$ value often appears. For example, Lewellen defines his characteristic length as,

$$\Lambda_o = 1.68\,\frac{u_*}{du/dz} = 1.68\,\frac{k_v z}{\phi_m(z/L)}, \tag{5}$$

where u_* is the friction velocity, du/dz is the vertical gradient of the horizontal windspeed, and ϕ_m is a diabatic influence function of momentum which is a dimensionless function of the ratio of the height (z) divided by the Monin-Obukhov length (L). I previously used this parameter for defining outer scale [Tofsted, 1992], though in hindsight it appears inappropriate. Zhao [1994],

and Finardi *et al.* [1995], use a form of the mixing length scale developed by Blackadar [1962]:

$$\frac{1}{\Lambda_o} = \frac{1}{\Lambda_\infty} + \frac{1}{k_v z}, \tag{6}$$

where Λ_∞ is the asymptotic value of Λ_o at large height. However, in no instance is this result linked to a turbulence spectrum. Hence, applications requiring an outer scale should look to other sources to determine this quantity.

Such a source seems to be exclusively available through data illustrated in or derived from Kaimal *et al.* [1972]. Nevertheless, use of this information is complicated by the mode of presentation of the data. Optical turbulence work usually involves integration of 3-D spectra, but the Kansas experimental data presented by Kaimal involves one-dimensional (1-D) spectra. Hence, to use the Kaimal data a turbulence spectrum must be posited, and then this spectrum must be converted to a 1-D representation. This task is treated in the following section. This reference can also be found along with many of the other articles cited in this report in the SPIE Milestone series compilation - *Turbulence in a Refractive Medium*, Andreas [1990].

2.3 One- and Three-Dimensional Spectra

Within the optical turbulence research community the assumption of 3-D homogeneous and isotropic turbulence is typically made. This assumption is useful, though in most cases it is false. Hinze [1987] points out that homogeneous turbulence is only possible under decaying turbulence conditions. To ensure that the turbulence is maintained requires nonhomogeneous energy sources. Nevertheless, under most conditions the source terms generating additional turbulence are small. I thus adopt a locally homogeneous condition.

Theory also suggests that turbulence is not isotropic at $\kappa < 1/L_o$. However, again, while use of the isotropic assumption is not entirely appropriate, the largest deviations occur only at the lowest frequencies, and these lowest frequencies have the least effect on the optical properties normally studied. Therefore, from a tractability view and due to its minimal impact, an isotropic turbulence assumption will be adopted throughout this discussion. In general, though, we do not need to adopt a homogeneous turbulence assumption in order to study properties of the refractive index power spectrum. Further, it is generally assumed that turbulence has a vertically inhomogeneous structure. With these caveats made, I proceed with the general development, first considering the limitations of the von Kármán spectrum.

As was mentioned in the introduction, the refractive index spectrum is related to the autocorrelation function, $\Gamma_n(r)$. Or, more generally, for scalar property

ξ, the relationship between its autocorrelation function and its spectrum may be written as [Beland, 1993],

$$\Phi_\xi(\vec{\kappa}) = \left(\frac{1}{2\pi}\right)^3 \iiint_{-\infty}^{\infty} \Gamma_\xi(\vec{r}) \exp(i\vec{\kappa}\cdot\vec{r})\, d\vec{r}, \tag{7}$$

where $\vec{\kappa} = (\kappa_1, \kappa_2, \kappa_3)$, $\vec{r} = (x, y, z)$, and $i = \sqrt{-1}$.

The Fourier relation between Φ_ξ and Γ_ξ permits the writing of the inverse transform relation,

$$\Gamma_\xi(\vec{r}) = \iiint_{-\infty}^{\infty} \Phi_\xi(\vec{\kappa}) \exp(-i\vec{\kappa}\cdot\vec{r})\, d\vec{\kappa}, \tag{8}$$

When the assumption of isotropy is invoked these equations may be reëxpressed in spherical coordinates and integrated over their spherical angular coordinates first, leaving functions dependent only on the magnitudes $\kappa = |\vec{\kappa}|$ and $r = |\vec{r}|$.

$$\Phi_\xi(\kappa) = \left(\frac{1}{2\pi}\right)^3 \int_0^{\infty} \Gamma_\xi(r)\, \frac{\sin(\kappa r)}{\kappa r}\, 4\pi r^2\, dr, \tag{9}$$

$$\Gamma_\xi(r) = \int_0^{\infty} \Phi_\xi(\kappa)\, \frac{\sin(\kappa r)}{\kappa r}\, 4\pi\kappa^2\, d\kappa. \tag{10}$$

Most atmospheric optics calculations are made in terms of weighted integrals involving Φ_n. But the refractive index is a function of temperature, pressure, and humidity fluctuations in the atmosphere, with temperature fluctuations being the dominant effect for visible to infrared frequencies. To measure these fluctuations directly usually involves tower measurements which record the temporally fluctuating properties of the atmosphere as the wind advects positionally varying air through the sensor mast location. Taylor's [1938] frozen turbulence hypothesis is then used to relate the temporal fluctuations observed to spatial fluctuations through extrapolation based on the mean wind speed.

The temporal records of the tower data can be analyzed, but these data only represent 1-D spectra. These spectra are related to their 3-D counterparts through the relation [Panofsky and Dutton, 1984],

$$F_\xi(\kappa_1) = 2\int_0^{\infty} \Phi_\xi\left(\sqrt{\kappa_1^2 + \kappa_r^2}\right) 2\pi\kappa_r\, d\kappa_r, \tag{11}$$

where κ_r is a polar spatial frequency coordinate in the (κ_2, κ_3) plane, corresponding to spatial coordinates normal to the wind direction. Note also that F_ξ is only defined for positive κ_1 values. Due to Φ_ξ function symmetry about zero, results at negative κ_1 values are folded onto the positive portion of the axis. This approach leads to the factor of 2 in front of the integral in eq. (11).

2.3.1 Atmospheric Refractive Index

I now note that although ξ was used to denote an arbitrary scalar property of the atmosphere, a so-called conservative passive additive, our real interest is in fluctuations of the atmospheric refractive index. Optical turbulence is caused by fluctuations in this index about its mean value. The mean refractive index is a function of air temperature, pressure, and humidity. Positional changes in these properties alter the refractive index of the atmosphere (n).

In fact, n is so close to unity in the atmosphere that a secondary variable, N, the refractivity, is normally used to describe n's variability:

$$n = 1 + N \times 10^{-6}. \tag{12}$$

The functional dependence of N is given in terms of its dry air behavior in combination with water vapor effects [Hill *et al.*, 1980],

$$N = N_{dry} + N_{vapor}, \tag{13}$$

$$N_{dry} = 0.3789 \times \left[1 + (5.337 - 0.0157\,T)\,P_t \times 10^{-6}\right] \frac{P_t\,N_0}{T}, \tag{14}$$

where P_t is the air pressure in torr, and T is the air temperature in Kelvin (K). N_0 expresses the wavelength dependence, given by,

$$N_0 = 64.328 + \frac{29498.1}{(146 - \lambda^{-2})} + \frac{255.4}{(41 - \lambda^{-2})}, \tag{15}$$

where λ (μm) is the radiation wavelength in the visible through far infrared band.

The water vapor influence on the refractive index is given by,

$$N_{vapor} = -0.0059 \times \left(1 - 0.0109\,\lambda^{-2}\right) A, \tag{16}$$

where A is the absolute humidity (g/m^3).

At visible through far infrared wavelengths, although there are humidity and pressure dependencies, temperature variations tend to clearly dominate the fluctuations in the refractive index about its mean. A secondary correlation between temperature and humidity fluctuations has been characterized by Wesely [1976], though the main correlation effect can be accounted for through use of the Bowen ratio [Kunkel and Walters, 1983]. These temperature fluctuations are driven largely by the energy flux of sensible heat at the earth's surface [Oke, 1978].

To quantify the variations in refractive index due to temperature, we write the differential of n with respect to temperature,

$$dn = dN \times 10^{-6} \approx -78.2 \times 10^{-6} \frac{P}{T^2}\,dT, \tag{17}$$

where pressure, P, has been converted to units of millibars (mbar) (1 torr = 1.33322 mbar). The important aspect to be emphasized here is that fluctuations in refractive index are directly proportional to fluctuations in temperature. We can thus equivalently study either a turbulent field of temperature fluctuations or refractive index fluctuations, and we will be studying the same phenomenon.

To directly study these fluctuations, the refractive index is normally rewritten as an average quantity, n_0, and a fluctuation component, n'.

$$n = n_0 + n'. \tag{18}$$

There are no optical turbulence effects due to n_0, while the n' statistic was previously discussed in connection with the autocorrelation function, $\Gamma_n(r)$.

2.3.2 Template Three-Dimensional Spectra

Hence temperature and refractive index fluctuations are strongly coupled, and once the structure of the temperature spectrum is understood, the refractive index spectrum immediately follows, having the same form. The difficulty remains, however, in determining an appropriate 3-D spectrum when only 1-D measurement data are available.

To solve this problem a family of template 3-D spectra will be used. These can be transformed into 1-D spectra and analyzed with respect to available empirical curves and data reported in the literature. This family of functions has the form,

$$\Upsilon_m(\kappa, \mathcal{L}) = \frac{\mathcal{L}^{11/3}\,(\kappa\mathcal{L})^{2m}}{\left[1+(\kappa\mathcal{L})^2\right]^{(11+6m)/6}}, \tag{19}$$

such that for $\kappa \gg \mathcal{L}$, $\Upsilon_m(\kappa, \mathcal{L}) \to \kappa^{-11/3}$. Based on this family, the standard von Kármán spectrum [Tatarskii, 1971] of turbulence can be written, using the $m = 0$ member of this family, as,

$$\Phi_{nV}(\kappa) = \beta_n\, C_n^2\, \Upsilon_0(\kappa, \mathcal{L}_o)\,. \tag{20}$$

where β_n is an exact form replacing the use of 0.033,

$$\beta_n = \frac{5}{36}\,\frac{2^{2/3}\Gamma(5/6)}{\pi^{3/2}\Gamma(2/3)} \approx 0.033. \tag{21}$$

In defense of Theodore von Kármán, I would note that it is arguable that he did not actually propose the spectrum honoring his name. von Kármán was certainly aware that the limiting behavior of turbulent spectra at low frequencies approaches a zero value at the origin. Hinze [1987] attributes the equivalent of Υ_1 to von Kármán [1948], while he attributes the use of Υ_0 to Saffman [1967]. All members of this family behave similarly at high spatial frequency κ, where they exhibit $\kappa^{-11/3}$ dependence. But at low spatial frequencies Υ_0 approaches a nonzero constant.

2.3.3 The Kaimal Curve

To study the behavior of this family in comparison to available data, the Υ_m functions were first transformed to 1-D spectra using eq. (11). These 1-D functions were then multiplied by frequency variable κ_1 so they could be compared to a 'universal' empirical curve suggested by Kaimal *et al.* [1972]. This equation was most recently expressed by Kaimal and Finnegan [1994] in the form,

$$\frac{f\,S_\xi(f)}{\sigma_\xi^2} = \frac{B\,(f/f_0)}{1 + B\,(f/f_0)^{5/3}}, \tag{22}$$

where ξ is the property under study (temperature, humidity, etc.), σ_ξ^2 is the variance of this property, $S_\xi(f)$ represents the 1-D spectral content of the fluctuating portion of this property expressed in terms of a unitless temporal frequency variable f, B is an empirically fit constant, and the parameter f_0 is related to the peak frequency, f_m. In their original paper, Kaimal *et al.* [1972] found $B = 0.16$. More recently, Kaimal and Finnegan [1994] report $B = 0.164$. This function is termed universal because Kaimal *et al.* viewed it as applicable to any scalar property. Hereafter, I shall refer to eq. (22) simply as the Kaimal curve.

In order to show the appropriateness of members of the template family in approximating the Kaimal curve, the Υ_m function 1-D versions were fitted to the asymptotic behaviors of the Kaimal curve at both high and low spatial frequency. The method of fitting involved shifting the transformed template function vertically through multiplication by a constant and horizontal shifting by multiplying the frequency variable by a scaling multiplier.

As an example, Υ_1, when converted to the Kaimal form, is expressed as,

$$\Psi_1(f') = \frac{0.6\,f'\,\left(f'^2 + 6/11\right)}{\left(1 + f'^2\right)^{11/6}}. \tag{23}$$

This form is fitted to the asymptotic behavior using $1.02045\,\Psi_1(0.47909\,f)$. The resulting fitted curves are plotted against the Kaimal curve in figure 1 for cases $m = 0$ to 3. As seen, the Υ_m functions exhibit peaks which are progressively narrower than the Kaimal curve.

In order to approximate the Kaimal curve using these template functions, it was realized that two of these functions could be combined in such a way that the asymptotic behavior remained the same, but the peak region could be better approximated.

Due to its incorrect limiting behavior at low frequency (it approaches a constant rather than zero) the Υ_0 function was not used. Having ruled out use of the Υ_0 function, the next two members of the Υ family were used:

$$\Phi_\alpha \propto A\,\Upsilon_1\,(\kappa,\,\mathcal{L}_a) + (1 - A)\,\Upsilon_2\,(\kappa,\,\mathcal{L}_b)\,, \tag{24}$$

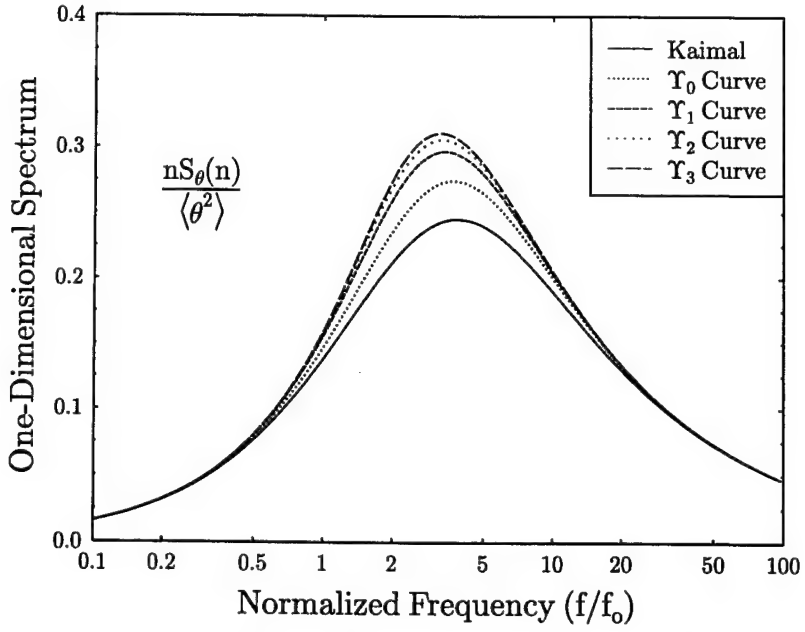

Figure 1. Fits of Υ_m functions to the asymptotic behavior of the proposed curve of Kaimal *et al.* [1972].

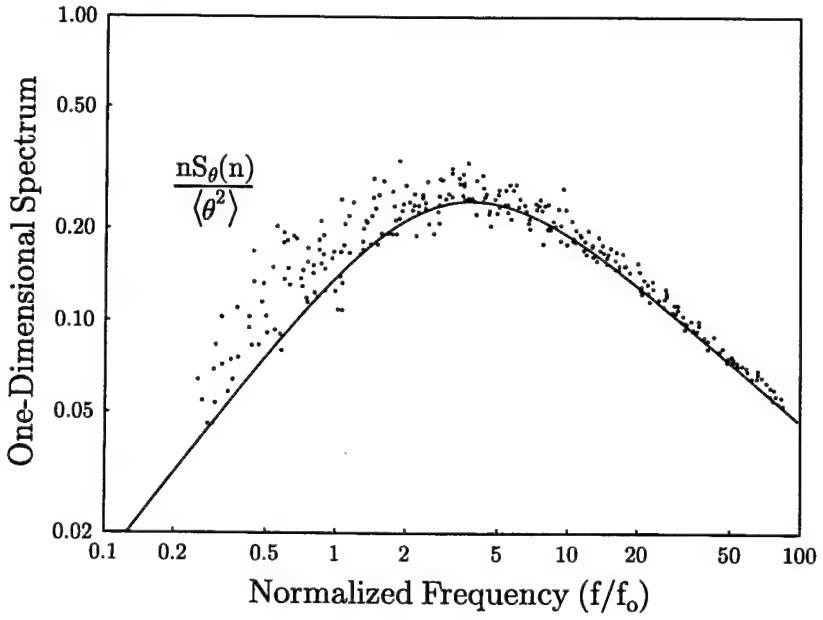

Figure 2. Comparison between Kansas experiment temperature fluctuation spectra data and Kaimal *et al.* [1972] empirical curve.

Figure 2 shows the data used in this analysis along with an empirical curve fit to this data as contained in figure 20 of Kaimal *et al.* [1972].

Mathematically, we can relate this comparison to a new form for the outer scale

influenced 3-D refractive index spectrum,

$$\Phi_n(\kappa) = \beta_n\, C_n^2 \left[\frac{A_1\, (\kappa\, \mathcal{L}_a)^2\, \mathcal{L}_a^{11/3}}{\left[1 + (\kappa\, \mathcal{L}_a)^2\right]^{17/6}} + \frac{(1 - A_1)\, (\kappa\, \mathcal{L}_b)^4\, \mathcal{L}_b^{11/3}}{\left[1 + (\kappa\, \mathcal{L}_b)^2\right]^{23/6}} \right]. \tag{25}$$

The $\mathcal{L}_a$ and $\mathcal{L}_b$ parameters appear as placeholders which are related to the peak frequency (f_m) of Kaimal *et al.* [1972] and have a direct relationship to the outer scale, but the exact nature of this relationship will only be obtained as a result of the analysis.

Using this form for the refractive index spectrum we may write the variance of refraction index fluctuations as,

$$\sigma_n^2 = \int_0^\infty \Phi_n(\kappa)\, 4\pi\, \kappa^2\, d\kappa = \frac{12\pi}{5}\, \beta_n\, C_n^2\, A_A \left[A_1 \left(\mathcal{L}_a^{2/3} - \frac{15}{17} \mathcal{L}_b^{2/3} \right) + \frac{15}{17} \mathcal{L}_b^{2/3} \right], \tag{26}$$

where A_A is an integration constant (see appendix),

$$A_A = \frac{\pi^{3/2}\, 3^{3/2}}{11\, \Gamma\left(\frac{5}{6}\right)\, \Gamma\left(\frac{2}{3}\right)}. \tag{27}$$

The 1-D spectrum for the refractive index can be generated from the 3-D spectrum through another integration (see appendix).

$$\begin{aligned} F_n(\kappa_1) &= 2 \int_0^\infty \Phi_n \left(\sqrt{\kappa_1^2 + \kappa_r^2} \right) 2\pi\, \kappa_r\, d\kappa_r \\ &= A_1\, \frac{12\pi}{5}\, \beta_n\, C_n^2\, \mathcal{L}_a^{5/3}\, \frac{\left[(\kappa_1\, \mathcal{L}_a)^2 + \frac{6}{11}\right]}{\left[1 + (\kappa_1\, \mathcal{L}_a)^2\right]^{11/6}} \\ &\quad + (1 - A_1)\, \frac{12\pi}{5}\, \beta_n\, C_n^2\, \mathcal{L}_b^{5/3}\, \frac{\left[(\kappa_1\, \mathcal{L}_b)^4 + \frac{12}{11}\, (\kappa_1\, \mathcal{L}_b)^2 + \frac{72}{187}\right]}{\left[1 + (\kappa_1\, \mathcal{L}_b)^2\right]^{17/6}}. \end{aligned} \tag{28}$$

Spherical symmetry of the spectrum, Φ_n, is assumed such that the integral results at negative κ_1 can be combined with positive κ_1 results, producing a one-sided spectrum containing only nonnegative values of κ_1. Hence, the factor 2 appears in front of the integral sign.

We now combine the results of the previous calculations to produce the expression $\Psi_n(\kappa_1) = \kappa_1\, F_n(\kappa_1)/\sigma_n^2$. Due to the normalization by σ_n^2 quantities

β_n and C_n^2 divide out. The remaining expression is independent of the scalar variable being studied.

$$\frac{\Psi_n(\kappa_1)}{\kappa_1} = \frac{\mathcal{L}_a^{5/3}}{A_X} \frac{\left[(\kappa_1 \mathcal{L}_a)^2 + \frac{6}{11}\right]}{\left[1 + (\kappa_1 \mathcal{L}_a)^2\right]^{11/6}} + \frac{\mathcal{L}_b^{5/3}\,(1 - A_1)}{A_1\, A_X} \frac{\left[(\kappa_1 \mathcal{L}_b)^4 + \frac{12}{11}(\kappa_1 \mathcal{L}_b)^2 + \frac{72}{187}\right]}{\left[1 + (\kappa_1 \mathcal{L}_b)^2\right]^{17/6}}, \tag{29}$$

where,

$$A_X = A_A \left[\mathcal{L}_a^{2/3} + \frac{15}{17}\left(\frac{1}{A_1} - 1\right)\mathcal{L}_b^{2/3}\right] \tag{30}$$

This expression is written in terms of the variable κ_1, while the Kaimal equation is written in terms of the variable f. κ_1 is a spatial frequency representation along the x axis which is normally understood as the direction of mean wind flow in meteorological studies. The f variable is a dimensionless temporal frequency variable related to tower sensed meteorological data. The two are related through the equation, $\kappa_1 z = 2\pi f$, where z is the height above the surface. To permit comparison let us define the variable κ_0 analogous to f_0, such that $\kappa_0 = 2\pi f_0/z$. Eq. (22) may therefore be rewritten in terms of the dimensionless frequency ratio $\kappa_1/\kappa_0 = f/f_0$,

$$\frac{\Psi_n(\kappa_1)}{\kappa_1} \approx \frac{B/\kappa_0}{1 + B\,(\kappa_1/\kappa_0)^{5/3}}. \tag{31}$$

The behavior of the $\Psi(\kappa_1)/\kappa_1$ function must thus obey B/κ_0 dependence at low frequency and $\kappa_1^{-5/3}\kappa_0^{2/3}$ dependence at high frequency.

Considering the high frequency behavior, cancellation results in an expression for κ_0 as a function of A_1 and A_X:

$$\kappa_0^{2/3} = \frac{1}{A_1\, A_X}. \tag{32}$$

Rewriting this expression, we have the condition:

$$\frac{1}{A_A} = A_1\,(\mathcal{L}_a\kappa_0)^{2/3} + \frac{15}{17}\,(1 - A_1)\,(\mathcal{L}_b\kappa_0)^{2/3}. \tag{33}$$

At the low frequency limit we obtain the expression,

$$\frac{B}{\kappa_0} = \frac{\left[\frac{6}{11}\,A_1\,\mathcal{L}_a^{5/3} + \frac{72}{187}\,(1 - A_1)\,\mathcal{L}_b^{5/3}\right]}{A_1\, A_X}. \tag{34}$$

The denominator on the right is just $\kappa_0^{-2/3}$. Eq. (34) then becomes,

$$\frac{11}{6}B = A_1 \left(\mathcal{L}_a \kappa_0\right)^{5/3} + \frac{12}{17}\left(1 - A_1\right)\left(\mathcal{L}_b \kappa_0\right)^{5/3}. \tag{35}$$

We thus have two equations in four variables: A_1, $\mathcal{L}_a$, $\mathcal{L}_b$, and κ_0. However, because of the relationships between $\mathcal{L}_a$, $\mathcal{L}_b$, and κ in eq. (25), and the definition given for the outer scale in eq. (4), we presume that $\mathcal{L}_a$, $\mathcal{L}_b$ must be proportional to the outer scale length L_o. κ_0 appears to perform a similar role in Kaimal's equation, except that it must be inversely proportional to L_o. Hence, the products $\mathcal{L}_a \kappa_0$ and $\mathcal{L}_b \kappa_0$ may be viewed as dimensionless functions which effectively displace their respective Υ functions along the κ axis. We then have only three unknowns ($\gamma_a = \mathcal{L}_a \kappa_0$, $\gamma_b = \mathcal{L}_b \kappa_0$, and A_1) in two equations. Conceptually, we might view A_1 as a free parameter which then defines γ_a and γ_b.

But there is a complication that arises when solving for an optimal value of A_1. From figure 1 it is observed that both Υ_1 and Υ_2 lie above the Kaimal curve. This means that the value of A_1 may not lie between 0 and 1 since what we wish to accomplish is to subtract a multiple of the upper curve (Υ_2) from a multiple of the lower curve (Υ_1), effectively pulling the Υ_1 line downward in the center toward the Kaimal curve and the Kansas data. This is only possible if A_1 is greater than unity. Unfortunately, when $A_1 > 1$ there is no general solution to both of these equations simultaneously for a general B value.

The best that can be hoped for is to try to approximately match the slope behavior given in eqs. (34) and (35), while choosing a value for A_1 that provides a good fit to either the available data or the Kaimal curve. Originally, I had conceived that it would be best to fit to the Kaimal curve, but this did not seem reasonable, particularly in view of the Kaimal curve's performance at low frequency. There, Kaimal *et al.* [1972] recommended a value for B of 0.16. Later, Kaimal and Finnegan [1994] amended this constant to $B = 0.164$. However, examining the data it appears that an asymptotic constant of $B = 0.20$ is a better fit.

In any case, the dispersion of the data is significantly larger at low frequencies than it is at high frequencies. It therefore makes sense that if only one curve can be solved for it should be the high frequency equation. Therefore, solving for γ_b in terms of A_1 and γ_a, we have,

$$\gamma_b = \left[\frac{17}{15}\frac{\left(\frac{1}{A_A} - A_1 \gamma_a^{2/3}\right)}{\left(1 - A_1\right)}\right]^{3/2}. \tag{36}$$

For the low frequency curve we have,

$$\gamma_b' = \left[\frac{17}{12}\frac{\left(\frac{11}{6}B - A_1 \gamma_a^{5/3}\right)}{\left(1 - A_1\right)}\right]^{3/5}. \tag{37}$$

Of interest is that we may choose a value for A_1 and then vary γ_a and look at a plot of the function $\gamma_b(A_1, \gamma_a) - \gamma_b'(A_1, \gamma_a)$ to see how this function varies. This difference approaches zero for a narrow range of γ_a values regardless of the value of A_1. Thus, although there is no solution to eqs. (34) and (35) in general, we may approach close to a solution and use this result. A relatively good choice of parameters that appears to come close to both the centroid of the data and fit for both high and low frequency limiting behaviors is $A_1 = 8.2$, $\gamma_a = 0.44$, $\gamma_b = 0.5254$. The γ_b result compares well with $\gamma_b' = 0.5221$, though it is not exactly equal. Figure 3 shows the resulting curve comparison with the Kansas data. As can be seen, the low frequency behavior of the proposed curve appears to fit to the centroid of the Kansas data better than the Kaimal curve of figure 2.

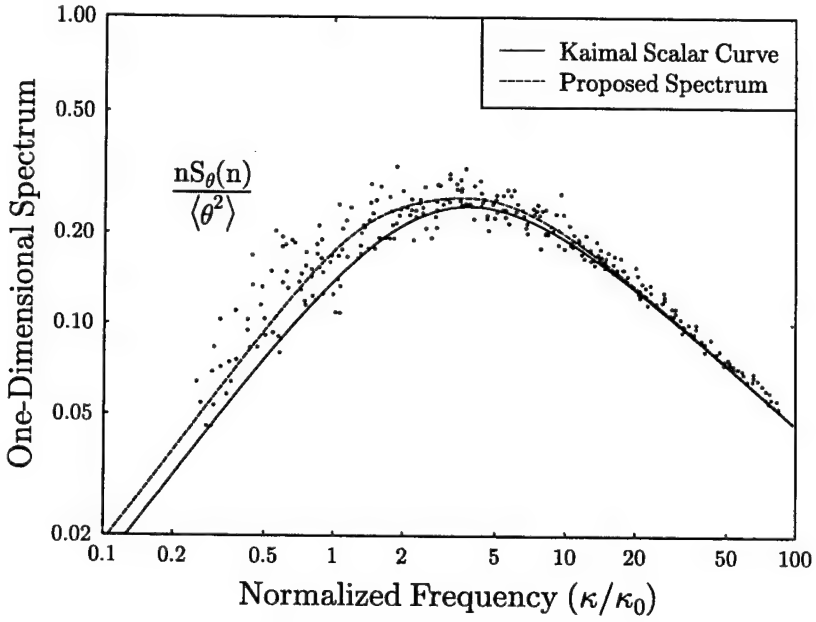

Figure 3. Comparison between the fitting method curve involving Υ_m functions, the Kaimal empirical curve, and Kansas data reported by Kaimal *et al.* [1972].

With these results, we may return to the description of the proposed 3-D refractive index spectrum in eq. (25). This equation can be rewritten in terms of β_n, C_n^2, κ_0, γ_a, and γ_b:

$$\Phi_n(\kappa) = \beta_n\, C_n^2\, \kappa_0^{-11/3} \left[\frac{A_1\, (\kappa\gamma_a/\kappa_0)^2\, \gamma_a^{11/3}}{\left[1 + (\kappa\gamma_a/\kappa_0)^2\right]^{17/6}} + \frac{(1 - A_1)\, (\kappa\gamma_b/\kappa_0)^4\, \gamma_b^{11/3}}{\left[1 + (\kappa\gamma_b/\kappa_0)^2\right]^{23/6}} \right]. \tag{38}$$

With A_1, γ_a, and γ_b fixed, β_n a constant, and C_n^2 constant for any given moment and location, the remaining parameters are κ and κ_0. Using the definition of

the outer scale in eq. (4), we find for the parameter values listed above,

$$\frac{\kappa_{\oslash}}{\kappa_0} \approx 4.71393; \qquad \kappa_0 \approx \frac{0.21214}{L_o}. \tag{39}$$

Writing the same result in terms of $\mathcal{L}_a$ and $\mathcal{L}_b$,

$$\kappa_0 \mathcal{L}_a = 0.4400 \quad \longrightarrow \quad \mathcal{L}_a = 2.0741\, L_o; \tag{40}$$

$$\kappa_0 \mathcal{L}_b = 0.5254 \quad \longrightarrow \quad \mathcal{L}_b = 2.4767\, L_o. \tag{41}$$

The resulting outer scale spectrum seen in figure 3 accurately models the refractive index spectrum to spectral frequencies well below the knee associated with $\kappa_{\oslash}$ (by approximately a factor of 5), thus significantly extending the simulation of the refractive index spectrum to very low wavenumbers. A plot of the outer scale region of the resulting 3-D spectrum is seen in figure 4.

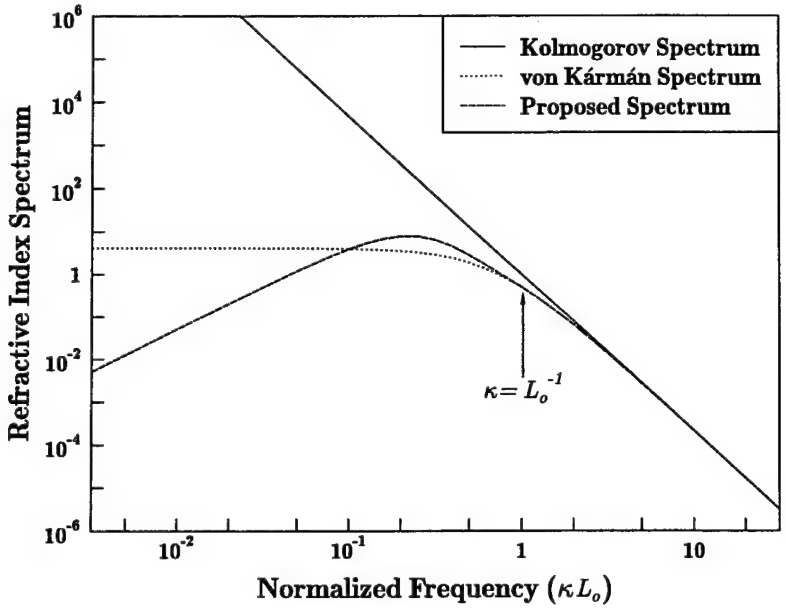

Figure 4. Outer scale portion of the proposed spectrum compared to the Kolmogorov and von Kármán spectrums.

In this figure the newly developed spectrum is compared with both the Kolmogorov and von Kármán spectrums. While the von Kármán spectrum rolls off to a constant value at low frequencies, the Kolmogorov spectrum increases to a singularity at zero frequency while the new spectrum rolls over toward a zero value at the origin. Of interest is a comparison between the von Kármán spectrum and the proposed spectrum. The von Kármán spectrum reaches a maximum at a frequency slightly below the outer scale frequency $\kappa_{\oslash}$ while the proposed spectrum continues to increase to a peak approximately twice that of the von Kármán spectrum.

2.4 Outer Scale Length

We are now in a position to discuss the association between the outer scale length and the frequency maximum measured during the 1968 Kansas experiment. In the previous section, we connected the outer scale length, L_o, to the κ_0 parameter. In this section, κ_0 is related to frequency maximum data collected during the 1968 Kansas experiment. This connection leads to a definition of outer scale as a function of similarity parameters in the atmospheric surface layer.

To build this connection, note that κ_0 is defined as $\kappa_0 = 2\pi f_0/z$. But f_0 is related to the frequency maximum, f_m, at which Kaimal's universal scalar curve peaks. This curve is given by,

$$F(f) = \frac{B\,(f/f_0)}{\left[1 + B\,(f/f_0)^{5/3}\right]}. \tag{42}$$

The peak of this curve is found by setting its derivative to zero. The location of the peak is denoted by f_m. Solving for this peak location we find,

$$f_0 = f_m \left(\frac{2B}{3}\right)^{3/5}. \tag{43}$$

For the original B value (0.160), $f_0 = 0.2611\, f_m$. For the revised value, $B = 0.164$, $f_0 = 0.2650\, f_m$. The two are relatively close, and since the Kaimal *et al.* [1972] analysis was based on the 0.160 value, we will use this result.

We have thus logically connected the outer scale value L_o to the frequency maximum location f_m. We find a functional form for f_m through an analysis of Kaimal *et al.*'s figure 18. The consolidated data from this figure are included in both figures 5 and 6 in this document. In these figures, the abscissa coordinate is the ratio z/L, representing the ratio of height above the surface (z) to the similarity parameter L known as the Monin-Obukhov length. The first of these figures (figure 5) presents f_m in a linear plot format as a function of z/L. The second figure (figure 6) presents f_m in log form as a function of z/L. Along with the data are two curves, one for $L < 0$ and one for $L > 0$. The distinction between these conditions is termed the stability:

$$f_m = \begin{cases} 0.460\sqrt{+\frac{z}{L}} + 0.0014 & \frac{z}{L} > 0; \\ 0.036\sqrt{-\frac{z}{L}} + 0.0014 & \frac{z}{L} < 0. \end{cases} \tag{44}$$

Negative L values correspond to daytime (unstable) conditions, where parcels of air displaced vertically tend to accelerate away from their level of origin. Positive

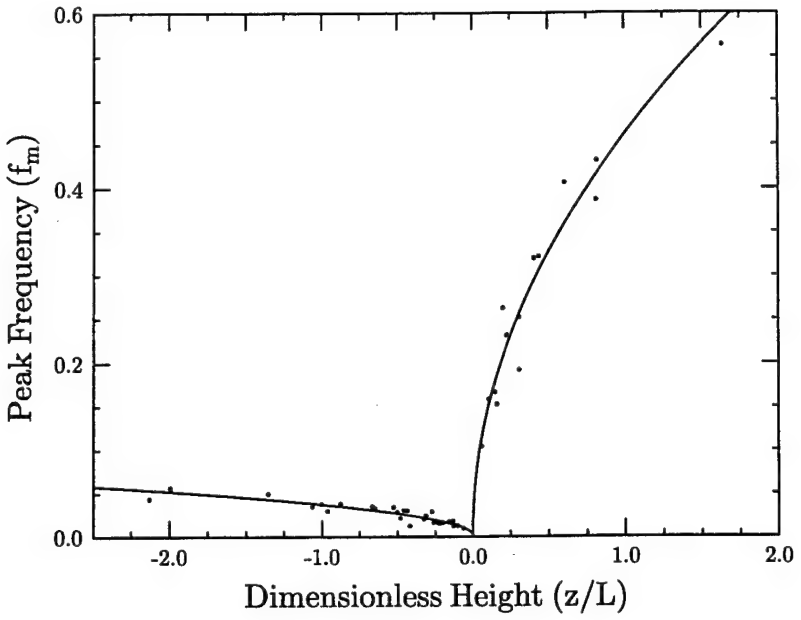

Figure 5. Comparison between the eq. (44) curve and frequency maximum data reported by Kaimal *et al.* [1972].

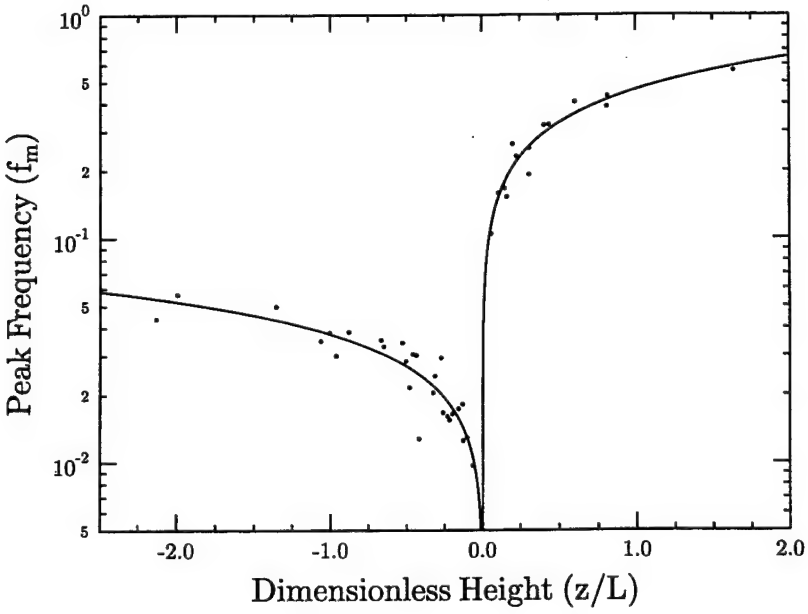

Figure 6. Comparison between the eq. (44) curve and frequency maximum data reported by Kaimal *et al.* [1972] with ordinate axis plotted on a log scale.

L values indicate stable conditions where air parcels tend to return to their level of origin.

Although Kaimal *et al.* [1972] included a hand drawn curve fit to the data, the

above relationship is also a reasonable fit. This functional relationship reveals several interesting features regarding outer scale dependencies within the surface layer atmosphere. First, it reveals that there are two pertinent length scales that affect the outer scale length. Focussing on the results for $B = 0.164$, we find, for nonnegligible heights, z,

$$L_o \approx \begin{cases} 0.281\sqrt{+z\,L} & L > 0,\ |z/L| > 0.1; \\ 3.592\sqrt{-z\,L} & L < 0,\ |z/L| > 0.1. \end{cases} \tag{45}$$

This functional relationship not only reveals that the outer scale depends on both the height and the Monin-Obukhov length, it also reveals that the dependence is equal between these two influencing variables. However, the outer scale exhibits considerably longer lengths under unstable atmospheric conditions than under stable conditions. Though this difference is likely due to bouyancy differences between the unstable daytime and the stable nocturnal surface layer atmospheres, the exact mechanism responsible for these differences cannot be discerned from this study.

Writing the full form of the f_m function,

$$L_o = \begin{cases} 0.281\,z/\left(\sqrt{+z/L} + 0.0030\right) & z/L > 0; \\ 3.592\,z/\left(\sqrt{-z/L} + 0.0389\right) & z/L < 0. \end{cases} \tag{46}$$

This form reveals explicitly how L_o is dependent on the Monin-Obukhov length. Both C_n^2 [cf., Rachele and Tunick, 1994] and the inner scale length, ℓ_o [cf., Tofsted and Auvermann, 1991] are also known to vary with atmospheric stability conditions. Hence, modeling atmospheric surface layer conditions will produce the parameters needed to predict the form of the refractive index spectrum as a function of height.

2.5 The Composite Spectrum

An application involving this new spectrum is as part of a calculation of the turbulent coherence diameter (chapter 3). Outer scale influences on the coherence diameter can be significant under certain circumstances. However, to evaluate the coherence diameter it is imperative that inner scale effects also be included. Therefore, it behooves one to modify the refractive index spectrum to include both inner and outer scale effects. Andrews and Phillips [1998] present several inner scale simulation functions, including their modified spectrum, the Tatarskii [1971] spectrum, and the Hill spectrum [Hill and Clifford, 1978].

These spectra will not be considered here in detail. Rather, I note that they typically either ignore outer scale effects altogether or simply replace the $\kappa^{-11/3}$ Kolmogorov dependence with a term associated with the von Kármán spectrum, $\left(\kappa_2 + \mathcal{L}^{-2}\right)^{-11/6}$. Inner scale effects are either represented as a series of terms as

in the Andrews and Phillips *modified* spectrum or as a superimposed multiplying factor riding on the main Kolmogorov dependence.

In either case, it is difficult to analytically evaluate the effects of both inner and outer scales because once the spectrum is represented as a single functional form it becomes difficult to integrate. Hence, I introduce here the *composite* spectrum. This new spectrum is composed of three parts. The first two of these parts represent a summation of two spectra, one representing only inner scale effects, the other only outer scale effects. The high frequency portion of the outer scale spectrum and the low frequency portion of the inner scale spectrum both reflect Kolmogorov behavior. The summation of these two spectra must therefore be balanced by the subtraction of a Kolmogorov spectrum from the sum. The spectrum thus produced includes both inner and outer scale effects while simultaneously permitting separate integration of the individual parts, avoiding, as much as possible, computational complexity.

This spectrum is written as:

$$\Phi_n(\kappa,\, \ell_o,\, L_o) = \Phi_{nO}(\kappa,\, L_o) + \Phi_{nI}(\kappa,\, \ell_o) - \Phi_{nK}(\kappa), \tag{47}$$

where $\Phi_{nK}(\kappa)$ is again the Kolmogorov spectrum (eq. (3)), the outer scale modified spectrum, Φ_{nO}, is synonymous with eq. (25), and

$$\Phi_{nI}(\kappa) = \beta_n\, C_n^2\, \kappa^{-11/3}\, F_F\left[V\left(\frac{\kappa\, \ell_o}{7.4}\right)\right], \tag{48}$$

is an approximation [Tofsted, 1991] to Frehlich's [2000] inner scale modified spectrum based on an analysis of measurement data, where,

$$V(x) = \log_{10}(x) + 0.72, \tag{49}$$

$$F_F(V) = \begin{cases} 1, & V < -3; \\ 1 + 0.424\, \exp\left(-2.725\, V^2\right), & -3 \le V < 0; \\ 0.712\, \left[1 + \cos\left(\frac{\pi V}{0.9}\right)\right]\, \left[1 - 0.786\, V^2\right] & 0 \le V < 0.9; \\ 0 & 0.9 \le V\ . \end{cases} \tag{50}$$

Although the value 7.4 appears in eq. (48) above as a constant, this quantity is actually somewhat variable. The ratio $\ell_o/7.4$ is supposed to represent the Kolmogorov microscale η, but the ratio between ℓ_o and η depends on the Prandtl number, which is itself temperature dependent [Hill, 1997].

An example of the behavior of the combined effects of inner and outer scale are seen in figure 7. In this figure, the spectrum has been normalized by dividing by the Kolmogorov spectrum. The inertial subrange portion of the spectrum thus evaluates to a constant value of unity in the curve's central section. The inner scale bump section is shown on the right hand portion of the curve and the outer scale section is seen on the left.

Though an outer scale value of 5 m was used, this value is not necessarily typical. Given the variability of outer scale on height and the Monin-Obukhov length, it is difficult to speak in generalities, yet, as is predicted by eq. (46), we should generally expect the width of the inertial subrange to be approximately an order of magnitude wider under daytime conditions than at night due to the functional difference in eq. (45) between stable and unstable conditions. Regarding the inner scale, figure 7 highlights the positions of two spatial frequencies related to the inner scale, ℓ_o, and the Kolmogorov microscale, η. The two are related through the equation, $\eta = \ell_o/7.4$ [Hill and Clifford, 1978], which also explains the appearance of the factor 7.4 in the argument to the V function of inner scale adjustment factor F_F.

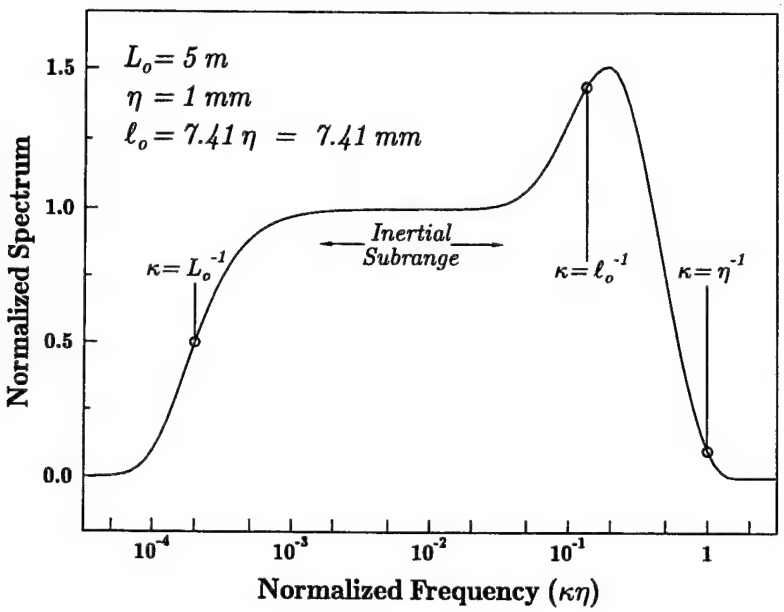

Figure 7. An example of normalized influences of inner and outer scale on a near surface refractive index spectrum.

As seen in the figure, the effects of the outer scale extend for approximately one-and-a-half decades. Inner scale effects have a similar extent. Hence, even though the inner-to-outer scale ratio is approximately a factor of 1000, there is still only about a decade and a half associated with the inertial subrange for this particular choice of inner and outer scale values. The effects of inner and outer scale are thus on the order of significance of the inertial subrange in this case.

The question may be asked whether this situation is typical. Studies of atmospheric effects on propagation often ignore inner and/or outer scale regions. The rationale for avoiding consideration of these effects most often concerns ease of computation. In the case of the proposed outer scale spectrum we have a form which is not necessarily easy to use, but which is nevertheless not intractable. The main question is whether such calculations are necessary and the answer is

likely that under most conditions the answer is no, for the simple reason that the outer scale may be so large (because of atmospheric conditions or the fact that the line of sight is sufficiently removed above the surface) that other factors, such as the weighting function used in performing integrations with respect to frequency, make the resulting calculations insensitive to spectral dependence on outer scale. Nevertheless, there will be certain conditions involving surface-to-surface propagation where both inner and outer scale influences on the optical turbulence parameterizations will be significant.

3. Turbulent Coherence Diameter

As an application, consider evaluation of the coherence diameter using the composite spectrum. The coherence diameter is given implicitly in the equation [Hill and Clifford, 1981],

$$1 = 4\pi^2 k^2 \int_0^S ds \int_0^\infty \left[1 - J_0\left(\frac{\kappa s r_o}{2.1 S}\right)\right] \Phi_n(\kappa, L_o(s), C_n^2(s), \ell_o(s))\, \kappa\, d\kappa, \quad (51)$$

where L_o, ℓ_o, and C_n^2 can all be functions of path position. In this equation, k is the radiation wavenumber $(2\pi/\lambda)$, s is a path position variable, S is the total path length, and r_o is the turbulent coherence diameter, often called the Fried coherence diameter [Fried, 1966].

Path position dependent parameters are most generally considered height dependent. Since the terrain underlying the path between object and observer is likely to be nonflat and/or a slant path, the values of these quantities will vary in nonlinear fashion. However, at a given moment for a given point along the optical path, the governing parameters can be considered constant. It is thus possible to directly evaluate the inner integral.

To evaluate this equation we begin by introducing the new length variable, $X = s r_o/(2.1 S)$. Using the composite spectrum introduced in the previous chapter, we may write eq. (51) as,

$$1 = 4\pi^2 k^2 \frac{S}{\rho_o} \int_0^{\rho_o} \beta_n C_n^2(XS/\rho_o) X^{5/3} [G(X, L_o) + H(X, \ell_o) - \aleph]\, dX, \quad (52)$$

where the path integration variable has been replaced by X, $\rho_o = r_o/2.1$, and G, H, and unity represent separate results for different components of the turbulence spectrum. G represents the combined outer scale effects, H represents the combined inner scale effects, subtraction by the constant $\aleph$ represents the Kolmogorov effect, and L_o and ℓ_o may vary as a function of range.

To solve for r_o involves an iterative method which requires an initial value of r_o to begin the search procedure. In general, r_o will be greater than this initial value, which is normally computed based on a Kolmogorov spectrum assumption.

3.1 Kolmogorov Spectrum Results

For the Kolmogorov portion of the spectrum, the inner integral may be written,

$$\beta_n C_n^2 \int_0^\infty [1 - J_0(\kappa X)] \kappa^{-11/3} \kappa \, d\kappa \approx 0.033 \times 1.11833 \, C_n^2 X^{5/3}. \quad (53)$$

The constant terms then combine as, $4\pi^2 \times 0.033 \times 1.11833 \approx 1.45695$. Through further analysis, we find that the integration constant, 1.11833, is actually the approximation of the expression,

$$\aleph = \frac{\pi}{2^{5/3}\,\Gamma(11/6)\,\Gamma(11/6)} \approx 1.118334400. \quad (54)$$

Returning to the main double integral in eq. (51), we have,

$$1 = 4\pi^2 k^2 \beta_n \aleph \int_0^S C_n^2 \left(\frac{s\, r_o}{2.1\, S}\right)^{5/3} ds, \quad (55)$$

which can be solved explicitly for r_o as,

$$r_o = 2.1 \left[\left(4\pi^2 \beta_n \aleph\right) k^2 S \int_0^1 C_n^2(S\, w)\, w^{5/3}\, dw \right]^{-3/5}, \quad (56)$$

where $w = s/S$ is a dimensionless path position variable and C_n^2 may vary as a function of range. This form corresponds to typical integral representations of the coherence diameter for the Kolmogorov refractive index spectrum [cf., Roddier, 1981].

One important factor to consider in the use of this equation regards the associated path position weighting function, $w^{5/3}$. In imaging problems, this weighting assumes the imager is located at range S ($w = 1$). In propagation problems (laser beams), this weighting function is normally reversed such that the laser source is located at the origin. In this case, a weighting function of $(1 - w)^{5/3}$ is used.

3.2 Outer Scale Spectrum Results

To evaluate the outer scale cases we now introduce three new dimensionless variables, $Y_a = \mathcal{L}_a/X$, $Y_b = \mathcal{L}_b/X$, and $u = \kappa X$. Given the spectral form

associated with the outer scale, evaluation of the inner integral in eq. (51) will involve the solving of equations having the form,

$$G_m(\mathcal{L}/X) = X^{-5/3} \int_0^\infty [1 - J_0(\kappa X)]\ \Upsilon_m(\kappa,\, \mathcal{L})\, \kappa\, d\kappa$$

$$= G_m(Y) = Y^{11/3} \int_0^\infty [1 - J_0(u)]\ \frac{(uY)^{2m}}{[1 + (uY)^2]^{m+11/6}}\, u\, du. \qquad (57)$$

Thus, the factor $X^{5/3}$ sifts out of these equations just as it does from the Kolmogorov expression.

After considerable math, it can be shown that,

$$G_1\,(Y_a) = Y_a^{11/3} \int_0^\infty [1 - J_0(u)]\ \frac{(uY_a)^2}{[1 + (uY_a)^2]^{17/6}}\, u\, du = \frac{18}{55}\, Y_a^{5/3}$$

$$+\frac{18}{55}\, \frac{2^{1/6}}{\Gamma\left(\frac{5}{6}\right)\, Y_a^{1/6}} \left[\frac{1}{2}\, K_{1/6}\left(\frac{1}{Y_a}\right) - Y_a\, K_{5/6}\left(\frac{1}{Y_a}\right)\right]. \qquad (58)$$

It can also be shown that in the limit of large Y_a,

$$G_1\,(Y_a) = Y_a^{11/3} \int_0^\infty [1 - J_0(u)]\ \frac{(uY_a)^2}{[1 + (uY_a)^2]^{17/6}}\, u\, du \approx \aleph - \frac{54}{55} Y_a^{-1/3}. \qquad (59)$$

For the second function we find the following results:

$$G_2\,(Y_b) = Y_b^{11/3} \int_0^\infty [1 - J_0(u)]\ \frac{(uY_b)^4}{[1 + (uY_b)^2]^{23/6}}\, u\, du = \frac{216}{935}\, Y_b^{5/3}$$

$$+\frac{216}{935}\, \frac{2^{1/6}}{\Gamma\left(\frac{5}{6}\right)\, Y_b^{1/6}} \left[\frac{23}{24}\, K_{1/6}\left(\frac{1}{Y_b}\right) - \left(Y_b + \frac{1}{8\, Y_b}\right)\, K_{5/6}\left(\frac{1}{Y_b}\right)\right]. \qquad (60)$$

In the limit of large Y_b for this function we find,

$$G_2\,(Y_b) = Y_b^{11/3} \int_0^\infty [1 - J_0(u)]\ \frac{(uY_b)^4}{[1 + (uY_b)^2]^{23/6}}\, u\, du \approx \aleph - \frac{972}{935} Y_b^{-1/3}. \qquad (61)$$

In these results, the functions $K_\nu(x)$ are modified Bessel functions of the second kind, order ν [cf., Kreyszig, 1972]. However, the raw integration results are

expressed in terms of modified Bessel functions of the first kind, $I_\nu(x)$, which are related to functions of the second kind through the relation,

$$K_\nu(x) = \frac{\pi}{2\,\sin(\nu\pi)}\,[I_{-\nu}(x) - I_\nu(x)]\,. \tag{62}$$

These calculations also involve use of the recurrence relationship,

$$I_\nu(x) = I_{\nu-2}(x) - \frac{2\nu}{x}\,I_{\nu-1}(x), \tag{63}$$

and the series expansion form of $I_\nu(x)$,

$$I_\nu(x) = \sum_{m=0}^{\infty} \frac{x^{2m+\nu}}{2^{2m+\nu}\,m!\,\Gamma(m+\nu+1)}. \tag{64}$$

Combining these effects, we generate the function,

$$G(Y_a,\,Y_b) = A_1\,G_1(Y_a) + (1 - A_1)\,G_2(Y_b). \tag{65}$$

Let $Y = L_o/X$. At large Y we have,

$$G(Y) \approx \aleph - 0.78078\,Y^{-1/3}. \tag{66}$$

The general solution is plotted in figure 8. In this figure the approximation function was used for Y values greater than 100 due to numerical stability problems encountered in evaluating the Bessel functions at high argument values. The approximation at this level is accurate to 5 digits of accuracy.

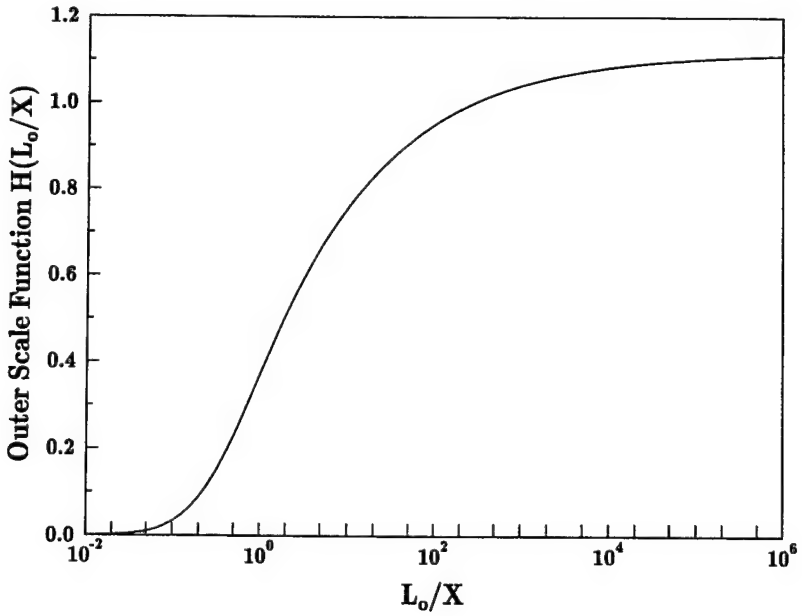

Figure 8. Outer scale influence function for the coherence diameter, plotted with respect to the parameter $Y = L_o/X$.

3.3 Inner Scale Spectrum Results

The results for the inner scale effects must generally be evaluated numerically due to the form used in describing the inner scale modifier to the spectrum. But the form of this calculation is essentially similar to the one made for the outer scale,

$$H(\ell_o/X) = X^{-5/3} \int_0^\infty [1 - J_0(\kappa X)]\, \kappa^{-8/3}\, F_F\left[V\left(\frac{\kappa \ell_o}{7.4}\right)\right] d\kappa \qquad (67)$$

This calculation can be written as a function of the dimensionless variable $Z = \ell_o/X$. The results of these calculations are shown in figure 9.

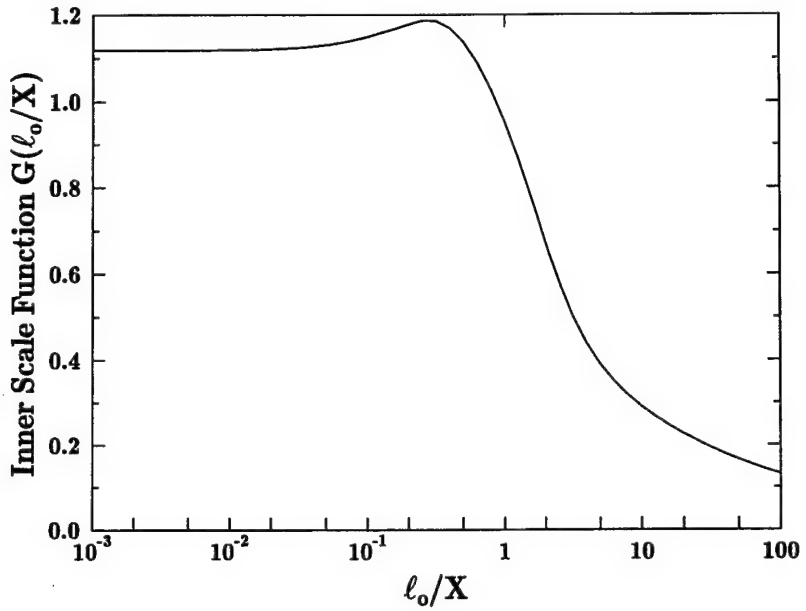

Figure 9. Inner scale influence function for the coherence diameter, plotted with respect to the parameter $Z = \ell_o/X$.

To study the behavior of this function at large Z we perform the change of variables $u = \kappa X$,

$$H(Z) = \int_0^{11.4/Z} [1 - J_0(u)]\, u^{-8/3}\, F_F\left[V\left(\frac{u\,Z}{7.4}\right)\right] du. \qquad (68)$$

The upper limit on this integration is due to the upper cutoff of the bump spectrum function F_F combined with the definition of the V function. For large Z the limits of the integration will become small, to the point that the quantity $[1 - J_0(u)]\, u^{-8/3}$ can be approximated by $u^{-2/3}/4$, using only the first two terms of the Bessel function expansion.

Considering the behavior of this portion of the integrand, and considering that the F_F function is almost constant throughout its nonzero range, it should perhaps come as no surprise that the integral evaluates approximately as $3u^{1/3}/4$ with an upper limit proportional to $1/Z$. Analysis of calculated integration results for $10^1 < Z < 10^3$ yields a functional form of approximately,

$$H(Z) \approx 0.61068\, Z^{-1/3}, \quad Z \gg 1. \tag{69}$$

This result is used to evaluate the $H(Z)$ at Z values where numerical techniques fail due to integration difficulties near the singularity at $u = 0$.

4. Conclusions

In this report, the modeling of outer scale effects on optical turbulence within the atmospheric surface layer has been considered. We first discussed the means used in treating outer scale effects by previous investigators. We considered prior limitations in the definition of outer scale and in the use of the standard von Kármán spectrum. A new definition of outer scale was given such that a particular point in the energy-containing-eddy region of the refractive index spectrum is used to denote the outer scale wavenumber, $\kappa_{\odot}$. A development was also described which relates outer scale effects on the refractive index spectrum to the research results of Kaimal *et al.* [1972] and a subsequent reanalysis by Kaimal and Finnegan [1994]. These results link the outer scale value to frequency maximum data for temperature fluctuations in the surface layer atmosphere. Analysis of this data and the subsequently proposed dimensionless height (z/L) parameterization of the frequency maximum (f_m) indicates that the outer scale is not merely a function of height above the surface, as has been commonly assumed, but rather is a function of height and the Monin-Obukhov length, firmly establishing that the outer scale is a function of both of the length parameters associated with the surface layer. As part of this analysis, a new outer scale influenced spectrum was developed which avoids the zero limit problem of the von Kármán spectrum. Lastly, the implications of the outer scale were considered in combination with inner scale effects within a proposed *composite* refractive index spectrum. The resulting spectrum permits the separable evaluation of inner and outer scale effects on atmospheric propagation. As an application, we considered the evaluation of the turbulent coherence diameter based on this new spectral model.

References

Andreas, E.L., ed., 1990, *Selected Papers on Turbulence in a Refractive Medium*, SPIE Optical Engineering Press, Bellingham, WA.

Andrews, L.C., and R.L. Phillips, 1998, *Laser Beam Propagation through Random Media*, SPIE Optical Engineering Press, Bellingham, WA.

Andrews, L.C., 1992, "An analytical model for the refractive index power spectrum and its application to optical scintillations in the atmosphere," *J. Mod. Opt.*, **39**:1849-1853.

Beland, R.R., 1993, "Propagation through Atmospheric Optical Turbulence," chapter 2 of volume 2 of *The Infrared & Electro-Optical Systems Handbook, Atmospheric Propagation of Radiation*, F.G. Smith, ed., SPIE Optical Engineering Press, Bellingham, WA, pp. 157-232.

Blackadar, A.K., 1962, "Vertical Distribution of Wind and Turbulent Exchange in a Neutral Atmosphere," *J. Geophys. Res.*, **67**:3095.

Churnside, J.H., 1990, "A spectrum of refractive-index turbulence in the turbulent atmosphere," *J. Mod. Opt.*, **37**:13-16.

Clifford, S.F., 1978, "The Classical Theory of Wave Propagation in a Turbulent Medium," chapter 2 of *Laser Beam Propagation in the Atmosphere*, J.W. Strohbehn, ed., Springer-Verlag, Berlin.

Davis, C.A., and D.L. Walters, 1994, "Atmospheric inner-scale effects on normalized irradiance variance," *Appl. Opt.*, **33**:8406-8411.

Ellerbroek, B.L., 1997, "Including outer scale effects in zonal adaptive optics calculations," *Appl. Opt.*, **36**:9456-9467.

Finardi, S., F. Trombetti, F. Tampieri, G. Brusasca, 1995, "An Assessment of Mixing-Length Closure Schemes for Models of Turbulent Boundary Layers over Complex Terrain," *Boundary Layer Meteorology*, **73**:343-356.

Frehlich, R., 1992, "Laser scintillation measurements of the temperature spectrum in the atmospheric surface layer," *J. Atmos. Sci.*, **49**:1494-1509.

Frehlich, R., 2000, "Simulation of laser propagation in a turbulent atmosphere," *Appl. Opt.*, **39**:393-397.

Frenzen, P., and C.A. Vogel, 1995, "On the Magnitude and Apparent Range of Variation of the von Karman Constant in the Atmospheric Surface Layer," *Boundary Layer Meteorol.*, **72**:371-392.

Fried, D.L., 1966, "Optical Resolution Through a Randomly Inhomogeneous Medium for Very Long and Very Short Exposures," *J Opt Soc Am*, **56**:1372-1379.

Gaskill, J.D., 1978, *Linear Systems, Fourier Transforms, and Optics*, J. Wiley & Sons, Inc., New York, NY.

Goodman, J.W., 1985, *Statistical Optics*, J. Wiley & Sons, Inc., New York, NY.

Gradshteyn, I.S., and I.M. Ryzhik, 1980, *Table of Integrals, Series, and Products*, translated and edited by Alan Jeffrey, Academic Press, Inc., Orlando, FL.

Hill, R.J., 1978, "Models of the scalar spectrum for turbulent advection," *J. Fluid Mech.*, **88**:541-562.

Hill, R.J., and S.F. Clifford, 1978, "Modified Spectrum of Atmospheric Turbulence Fluctuations and Its Application to Optical Propagation," *J Opt Soc Am*, **68**:892-899.

Hill, R.J., S.F. Clifford, and R.S. Lawrence, 1980, "Refractive Index and Absorption Fluctuations in the Infrared Caused by Temperature, Humidity, and Pressure Fluctuations," *J. Opt. Soc. Am.*, **70**:1182-1205.

Hill, R.J., and S.F. Clifford, 1981, "Theory of saturation of optical scintillation by strong turbulence for arbitrary refractive-index spectra," *J. Opt. Soc. Am.*, **71**:675-686.

Hill, R.J., 1997, "Algorithms for obtaining atmospheric surface-layer fluxes from scintillation measurements", *J. Atmos. Oceanic Technol.*, **14**:456-467.

Hinze, J.O., 1987, *Turbulence*, McGraw-Hill Inc., New York, NY.

Ishimaru, A., 1978, *Wave Propagation and Scattering in Random Media, Volume 2: Multiple Scattering, Turbulence, Rough Surfaces, and Remote Sensing*, Academic Press, New York, NY.

Kaimal, J.C., J.C. Wyngaard, Y. Izumi, and O.R. Coté, 1972, "Spectral characteristics of surface-layer turbulence," *Quarterly Journal of the Royal Meteorological Society*, **98**:563-589.

Kaimal, J.C., and J.J. Finnegan, 1994, *Atmospheric Boundary Layer Flows, Their Structure and Measurement*, Oxford University Press, New York, NY.

Kopeika, N.S., 1998, *A System Engineering Approach to Imaging*, SPIE Optical Engineering Press, Bellingham, WA.

Kolmogorov, A.N., 1962, "A refinement of previous hypotheses concerning the local structure of turbulence in a viscous incompressible fluid at high Reynolds number," *J. Fluid Mech.*, **13**:82-85.

Kreyszig, E., 1972, *Advanced Engineering Mathematics*, J. Wiley and Sons, Inc., New York, NY.

Kunkel, K.E., and D.L. Walters, 1983, "Modeling the Diurnal Dependence of the Optical Refractive Index Structure Parameter," *J. Geoph. Res.*, **88**:10,999-11,004.

Lewellen, W.S., 1977, "Use of invariant modeling," chapter 9 of *Handbook of Turbulence*, W. Frost and T.H. Moulden, eds., Plenum, New York, NY.

Martin, J.M., and S.M. Flatté, 1988, "Intensity images and statistics from numerical simulation of wave propagation in 3D random media," *Appl. Opt.*, **27**:2111-2126.

Nelson, D.H., D.L. Walters, E.P. MacKerrow, M.J. Schmitt, C.R. Quick, W.M. Porch, and R.R. Petrin, 2000, "Wave optics simulation of atmospheric turbulence and reflective speckle effects in CO_2 lidar," *Appl. Opt.*, **39**:1857-1871.

Oke, T.R., 1978, *Boundary Layer Climates*, Methuen & Co. Ltd., London.

Panofsky, H.A., and J.A. Dutton, 1984, *Atmospheric Turbulence: models and methods for engineering applications*, J. Wiley & Sons, New York, NY.

Rachele, H., and A. Tunick, 1994, "Energy Balance Model for Imagery and Electromagnetic Propagation," *J. Appl. Meteorology*, **33**:964-976.

Roddier, F., 1981, "The Effects of Atmospheric Turbulence in Optical Astronomy," in *Progress in Optics Vol. XIX*, E.Wolf, ed., North-Holland.

Saffman, P.G., 1967, "Large-Scale Structure of Homogeneous Turbulence," *J. Fluid Mech.*, **27**:581.

Tatarskii, V.I., 1971, *The Effects of the Turbulent Atmosphere on Wave Propagation*, translated for NOAA by Israel Program for Scientific Translations, Jerusalem.

Taylor, G.I., 1938, "The spectrum of turbulence," *Proc. Roy. Soc. London*, **A164**:476-490.

Tofsted, D.H., 1991, *Baseline Resolution of Atmosphere Related FADEWS Modeling Issues, Volume 6, Scintillation Distribution, Part 1 - Theoretical Development*, ASL-TR-0304-1, US Army Atmospheric Sciences Laboratory, White Sands Missile Range, NM 88002-5501.

Tofsted, D.H., and H.J. Auvermann, 1991, *Baseline Resolution of Atmosphere Related FADEWS Modeling Issues, Volume 9, Additional Model Improvements*, ASL-TR-0302, US Army Atmospheric Sciences Laboratory, White Sands Missile Range, NM 88002-5501.

Tofsted, D.H., 1992, "Outer-scale effects on beam wander and angle-of-arrival variances," *Appl. Opt.*, **31**:5865-5870.

von Kármán, T., 1948, "Progress in the statistical theory of turbulence," *Proc. Natl. Acad. Sci. U.S.*, **34**:530-539.

Wesely, M.L., 1976, "The Combined Effect of Temperature and Humidity Fluctuations on Refractive Index," *J. Appl. Met.*, *bf 15*:43-49.

Yan, H., S. Li, D. Zhang, and S. Chan, 2000, "Numerical simulation of an adaptive optics system with laser propagation in the atmosphere," *Appl. Opt.*, **39**:3023-3031.

Young, C.Y., L.C. Andrews, and A. Ishimaru, 1998, "Time-of-arrival fluctuations of a space-time Gaussian pulse in weak optical turbulence: an analytic solution," *Appl. Opt.*, **37**:7655-7660.

Zhao, M., 1994, "A Planetary Boundary Layer Numerical Model Containing Third-Order Derivative Terms," *Boundary Layer Meteorology*, **69**:71-82.

Appendix
Integration Methods

In section 2.3.3 of this report, several integrations were performed. In this appendix the methods used in performing these integrations are described. The first of these operations is related to the Υ_m family of functions introduced in section 2.3.2. In 2.3.3, these functions must be integrated into one-dimensional (1-D) form. Figure 1 contains a family of such integrated curves. Second, we integrate these functions to generate the variance statistic σ_n^2.

These integrations can all be performed using the 3.259.3 result from Gradshteyn and Ryzhik [1980] (hereafter, G&R):

$$\int_0^\infty x^{\lambda-1}\,(1+\alpha x^p)^{-\mu}\,(1+\beta x^p)^{-\nu}\,dx = \frac{1}{p}\,\alpha^{-\lambda/p}\,B\left(\frac{\lambda}{p},\,\mu+\nu-\frac{\lambda}{p}\right) \times\ {}_2F_1\left(\nu,\,\frac{\lambda}{p};\,\mu+\nu;\,1-\frac{\beta}{\alpha}\right); \qquad (A-1)$$

where $|\arg\,\alpha| < \pi$, $|\arg\,\beta| < \pi$, $p > 0$, and $0 < \Re\lambda < 2\Re(\mu+\nu)$. The function $B(x,y)$ is the beta function,

$$B(x,y) = \frac{\Gamma(x)\,\Gamma(y)}{\Gamma(x+y)}. \qquad (A-2)$$

The ${}_2F_1$ function is Gauss' hypergeometric function, given as,

$${}_2F_1(\alpha,\,\beta;\,\gamma;\,z) = 1 + \frac{\alpha\beta}{\gamma\cdot 1}z + \frac{\alpha\,(\alpha+1)\,\beta\,(\beta+1)}{\gamma\,(\gamma+1)\cdot 1\cdot 2}z^2 + \ldots \qquad (A-3)$$

In performing the evaluation of σ_n^2 begin by considering the integral,

$$\sigma_n^2 = \int_0^\infty \Phi_n(\kappa)\,4\pi\,\kappa^2\,d\kappa. \qquad (A-4)$$

Removing constant terms from the integral, we have two resulting integrations to perform:

$$\int_0^\infty \frac{(\kappa\,\mathcal{L}_a)^2\,\mathcal{L}_a^{11/3}}{\left[1+(\kappa\,\mathcal{L}_a)^2\right]^{17/6}}\,\kappa^2\,d\kappa = \mathcal{L}_a^{2/3}\int_0^\infty \frac{u^4}{\left[1+u^2\right]^{17/6}}\,du, \qquad (A-5)$$

where $u = \kappa\,\mathcal{L}_a$, and,

$$\int_0^\infty \frac{(\kappa\,\mathcal{L}_b)^4\,\mathcal{L}_b^{11/3}}{\left[1+(\kappa\,\mathcal{L}_b)^2\right]^{23/6}}\,\kappa^2\,d\kappa = \mathcal{L}_b^{2/3}\int_0^\infty \frac{u^6}{\left[1+u^2\right]^{23/6}}\,du, \qquad (A-6)$$

where $u = \kappa\,\mathcal{L}_b$.

We can write these two integrals in the more general form,

$$I(n) = \int_0^\infty \frac{x^{2n}}{(1+x^2)^{n+5/6}}\,dx \qquad (A-7)$$

This integral can be solved using the cited G&R formula where the following substitutions are introduced: $\alpha = \beta = 1$, $p = 2$, $\lambda = 2n+1$, $\mu = \nu$, $\mu + \nu = n + 5/6$. All the components here are real, and the final condition is met where $2n + 1 < 2n + 5/3$. Hence, we obtain the result,

$$I(n) = \frac{1}{2}\,\frac{\Gamma\left(n+\frac{1}{2}\right)\,\Gamma\left(\frac{1}{3}\right)}{\Gamma\left(n+\frac{5}{6}\right)}. \qquad (A-8)$$

Here, the hypergeometric function's main argument $(1 - \beta/\alpha)$ evaluates to zero, and hence the function itself evaluates to unity and drops out of the final expression.

To evaluate the transformation from three-dimensional (3-D) spectra to 1-D, we begin by considering the integral:

$$2\int_0^\infty \Phi_n\left(\sqrt{\kappa_1^2+\kappa_r^2}\right)\,2\pi\,\kappa_r\,d\kappa_r. \qquad (A-9)$$

Again, removing constants, we find the following two integrals at the heart of the problem:

$$\int_0^\infty \frac{\left(\kappa_1^2+\kappa_r^2\right)\,\mathcal{L}_a^2\,\mathcal{L}_a^{11/3}}{\left[1+\kappa_1^2\,\mathcal{L}_a^2+\kappa_r^2\,\mathcal{L}_a^2\right]^{17/6}}\,\kappa_r\,d\kappa_r = \mathcal{L}_a^{5/3}\int_0^\infty \frac{\left(v^2+u^2\right)}{\left[1+v^2+u^2\right]^{17/6}}u\,du, \qquad (A-10)$$

where $u = \kappa_r\mathcal{L}_a$ and $v = \kappa_1\mathcal{L}_a$; and,

$$\int_0^\infty \frac{\left(\kappa_1^2+\kappa_r^2\right)^2\,\mathcal{L}_b^2\,\mathcal{L}_b^{11/3}}{\left[1+\kappa_1^2\,\mathcal{L}_b^2+\kappa_r^2\,\mathcal{L}_b^2\right]^{23/6}}\,\kappa_r\,d\kappa_r = \mathcal{L}_b^{5/3}\int_0^\infty \frac{\left(v^2+u^2\right)^2}{\left[1+v^2+u^2\right]^{23/6}}u\,du; \qquad (A-11)$$

where $u = \kappa_r\mathcal{L}_b$ and $v = \kappa_1\mathcal{L}_b$. To simplify these integrals we can remove the v^2 dependence from the denominators:

$$\begin{aligned}\int_0^\infty \frac{\left(v^2+u^2\right)}{\left[1+v^2+u^2\right]^{17/6}}u\,du &= \frac{v^2}{\left[1+v^2\right]^{17/6}}\int_0^\infty \frac{u}{\left[1+A\,u^2\right]^{17/6}}\,du \\ &+ \frac{1}{\left[1+v^2\right]^{17/6}}\int_0^\infty \frac{u^3}{\left[1+A\,u^2\right]^{17/6}}\,du,\end{aligned} \qquad (A-12)$$

where $A = (1+v^2)^{-1}$; and,

$$\int_0^\infty \frac{\left(v^2+u^2\right)^2}{\left[1+v^2+u^2\right]^{23/6}} u\,du = \frac{v^4}{\left[1+v^2\right]^{23/6}} \int_0^\infty \frac{u}{\left[1+A\,u^2\right]^{23/6}}\,du + \frac{2v^2}{\left[1+v^2\right]^{23/6}} \int_0^\infty \frac{u^3}{\left[1+A\,u^2\right]^{23/6}}\,du + \frac{1}{\left[1+v^2\right]^{23/6}} \int_0^\infty \frac{u^5}{\left[1+A\,u^2\right]^{23/6}}\,du, \qquad (A-13)$$

where $A = (1+v^2)^{-1}$.

These forms are thus seen to devolve to the solution of the following general integral:

$$\int_0^\infty \frac{x^{2m+1}}{(1+A\,x^2)^{n+5/6}}\,dx, \qquad (A-14)$$

where $0 \le m \le n-1$. This form can also be solved using the previously mentioned G&R result. Here, we use $\lambda = 2m+2$, $p = 2$, $\alpha = \beta = A$, $\mu = \nu$, and $\mu + \nu = n + 5/6$. In general, we find a result,

$$\int_0^\infty \frac{x^{2m+1}}{(1+A\,x^2)^{n+5/6}}\,dx = \frac{1}{2}\,(1+v^2)^{(m+1)}\,\frac{\Gamma(m+1)\,\Gamma(n-m-1/6)}{\Gamma(n+5/6)}. \qquad (A-15)$$

Distribution

	Copies
NASA MARSHALL SPACE FLT CTR ATMOSPHERIC SCIENCES DIV E501 ATTN DR FICHTL HUNTSVILLE AL 35802	1
NASA SPACE FLT CTR ATMOSPHERIC SCIENCES DIV CODE ED 41 1 HUNTSVILLE AL 35812	1
US ARMY MISSILE CMND AMSMI RD AS SS ATTN MR H F ANDERSON REDSTONE ARSENAL AL 35898-5253	1
US ARMY MISSILE CMND AMSMI RD AS SS ATTN MR B WILLIAMS REDSTONE ARSENAL AL 35898-5253	1
US ARMY MISSILE CMND AMSMI RD DE SE ATTN MR GORDON LILL JR REDSTONE ARSENAL AL 35898-5245	1
US ARMY MISSILE CMND REDSTONE SCI INFO CTR AMSMI RD CS R DOC REDSTONE ARSENAL AL 35898-5241	1
US ARMY MISSILE CMND AMSMI REDSTONE ARSENAL AL 35898-5253	1
PACIFIC MISSILE TEST CTR GEOPHYSICS DIV ATTN CODE 3250 POINT MUGU CA 93042-5000	1
ATMOSPHERIC PROPAGATION BRANCH SPAWARSYSCEN SAN DIEGO D858 49170 PROPAGATION PATH SAN DIEGO CA 92152-7385	1
METEOROLOGIST IN CHARGE KWAJALEIN MISSILE RANGE PO BOX 67 APO SAN FRANCISCO CA 96555	1
NCAR LIBRARY SERIALS NATL CTR FOR ATMOS RSCH PO BOX 3000 BOULDER CO 80307-3000	1

HEADQUARTERS DEPT OF ARMY
DAMI POI
ATTN LEE PAGE
WASHINGTON DC 20310-1067 1

DEAN RMD
ATTN DR GOMEZ
WASHINGTON DC 20314 1

US ARMY INFANTRY
ATSH CD CS OR
ATTN DR E DUTOIT
FT BENNING GA 30905-5090 1

HQ AFWA/DNX
106 PEACEKEEPER DR STE 2N3
OFFUTT AFB NE 68113-4039 1

PHILLIPS LABORATORY
PL LYP
ATTN MR CHISHOLM
HANSCOM AFB MA 01731-5000 1

PHILLIPS LABORATORY
PL LYP 3
HANSCOM AFB MA 01731-5000 1

AFRL/VSBL
29 RANDOLPH RD
HANSCOM AFB MA 01731 1

ARL CHEMICAL BIOLOGY
NUC EFFECTS DIV
AMSRL SL CO
APG MD 21010-5423 1

US ARMY MATERIEL SYST
ANALYSIS ACTIVITY
AMSXY
APG MD 21005-5071 1

ARMY RESEARCH LABORATORY
AMSRL D
2800 POWDER MILL ROAD
ADELPHI MD 20783-1145 1

ARMY RESEARCH LABORATORY
AMSRL OP CI SD TL
2800 POWDER MILL ROAD
ADELPHI MD 20783-1145 1

ARMY RESEARCH LABORATORY
AMSRL CI LL
ADELPHI MD 20783-1197 1

ARMY RESEARCH LABORATORY
AMSRL SS SH
ATTN DR SZTANKAY
2800 POWDER MILL ROAD
ADELPHI MD 20783-1145 1

ARMY RESEARCH LABORATORY
AMSRL CI
ATTN J GANTT
2800 POWDER MILL ROAD
ADELPHI MD 20783-1197 1

ARMY RESEARCH LABORATORY
AMSRL
2800 POWDER MILL ROAD
ADELPHI MD 20783-1145 1

NATIONAL SECURITY AGCY W21
ATTN DR LONGBOTHUM
9800 SAVAGE ROAD
FT GEORGE G MEADE MD 20755-6000 1

US ARMY RSRC OFC
ATTN AMXRO GS DR BACH
PO BOX 12211
RTP NC 27009 1

DR JERRY DAVIS
NCSU
PO BOX 8208
RALEIGH NC 27650-8208 1

US ARMY CECRL
CECRL GP
ATTN DR DETSCH
HANOVER NH 03755-1290 1

US ARMY ARDEC
SMCAR IMI I BLDG 59
DOVER NJ 07806-5000 1

ARMY DUGWAY PROVING GRD
STEDP MT DA L 3
DUGWAY UT 84022-5000 1

ARMY DUGWAY PROVING GRD
STEDP MT M
ATTN MR BOWERS
DUGWAY UT 84022-5000 1

DEPT OF THE AIR FORCE
OL A 2D WEATHER SQUAD MAC
HOLLOMAN AFB NM 88330-5000 1

PL WE
KIRTLAND AFB NM 87118-6008 1

USAF ROME LAB TECH
CORRIDOR W STE 262 RL SUL
26 ELECTR PKWY BLD 106
GRIFFISS AFB NY 13441-4514 1

AFMC DOW
WRIGHT PATTERSON AFB OH 45433-5000 1

US ARMY FIELD ARTILLERY SCHOOL
ATSF TSM TA
FT SILL OK 73503-5600 1

US ARMY FOREIGN SCI TECH CTR
CM
220 7TH STREET NE
CHARLOTTESVILLE VA 22448-5000 1

NAVAL SURFACE WEAPONS CTR
CODE G63
DAHLGREN VA 22448-5000 1

US ARMY OEC
CSTE EFS
PARK CENTER IV
4501 FORD AVE
ALEXANDRIA VA 22302-1458 1

US ARMY CORPS OF ENGRS
ENGR TOPOGRAPHICS LAB
ETL GS LB
FT BELVOIR VA 22060 1

US ARMY TOPO ENGR CTR
CETEC ZC 1
FT BELVOIR VA 22060-5546 1

SCI AND TECHNOLOGY
101 RESEARCH DRIVE
HAMPTON VA 23666-1340 1

US ARMY NUCLEAR CML AGCY
MONA ZB BLDG 2073
SPRINGFIELD VA 22150-3198 1

USATRADOC
ATCD FA
FT MONROE VA 23651-5170 1

ATRC WSS R
WSMR NM 88002-5502 1

ARMY RESEARCH LABORATORY
AMSRL CI E
COMP & INFO SCI DIR
WSMR NM 88002-5501 1

DTIC
8725 JOHN J KINGMAN RD
STE 0944
FT BELVOIR VA 22060-6218 1

US ARMY MISSILE CMND
AMSMI
REDSTONE ARSENAL AL 35898-5243 1

US ARMY DUGWAY PROVING GRD
STEDP3
DUGWAY UT 84022-5000 1

USTRADOC ATCD FA FT MONROE VA 23651-5170	1
WSMR TECH LIBRARY BR STEWS IM IT WSMR NM 88002	1
US ARMY RESEARCH LAB AMSRL D DR D SMITH 2800 POWDER MILL RD ADELPHI MD 20783-1197	1
US ARMY CECOM INFORMATION & INTELLIGENCE WARFARE DIRECTORATE ATTN AMSEL RD IW IP FORT MONMOUTH NJ 07703-5211	1
ARMY RESEARCH LABORATORY AMSRL CI E ATTN D TOFSTED WSMR NM 88002-5501	21
Record copy	1
TOTAL	77